Fractal Graphene Patch Antennas and the THz Communications Revolution

Conference Paper *in* IOP Conference Series Materials Science and Engineering · February 2021

DOI: 10.1088/1757-899X/1060/1/012001

4 authors, including:

Albert Boretti

207 PUBLICATIONS **2,053** CITATIONS

SEE PROFILE

Lorenzo Rosa

Università degli Studi di Modena e Reggio Emilia

134 PUBLICATIONS **1,985** CITATIONS

SEE PROFILE

Stefania Castelletto

RMIT University

238 PUBLICATIONS **3,950** CITATIONS

SEE PROFILE

Fractal Graphene Patch Antennas and the THz Communications Revolution

Fractal Graphene Patch Antennas and the THz Communications Revolution

J M Blackledge[1], A Boretti[2], L Rosa[3] and S Castelletto[4]

[1]School of Electrical and Electronic Engineering, Technological University Dublin, Ireland; Department of Computer Science, University of Western Cape, South Africa; School of Mathematics, Statistics and Computer Science, University of KwaZulu-Natal, South Africa; Faculty of Arts, Science and Technology, Wrexham Glyndwr University of Wales, UK.
[2]Department of Mechanical Engineering, College of Engineering, Prince Mohammad Bin Fahd University, Al Khobar, Saudi Arabia.
[3]Department of Engineering 'Enzo Ferrari', University of Modena and Reggio Emilia, Modena, Italy and Applied Plasmonics Laboratory, Center for Micro-Photonics, Swinburne University of Technology, Australia.
[4]School of Engineering, Royal Melbourne Institute of Technology, Australia.

E-mail: [1]jonathan.blackledge@tudublin.ie

Abstract.

Fractal antennas have and are continuing to receive attention in regard to the future of wireless communications. This is because of their wide- and multi-band capabilities, the opportunity of fractal geometries to drive multiple resonances, and, the ability to make smaller and lighter antennas with fewer components and radiative elements with higher gains. Small scale (i.e. on the micro- and nano-scale) and ultra high frequency (in the Terahertz or THz range) fractal antennas composed of Graphene have the potential to enhance wireless communications at a data rate that is unprecedented, i.e. $\sim 10^{12}$ bits per second. A Fractal Graphene antenna is a high-frequency tuneable antenna for radio communications in the THz spectrum, enabling unique applications such as wireless nano-networks. This is because (mono-layer) Graphene is a one-atom-thick two-dimensional allotrope of Carbon with the highest known electrical conductivity that is currently unavailable in any other material, including metals such as Gold and Silver. Thus, combining the properties of Graphene with the self-affine characteristics of a fractal at the micro- and nano-scale, provides the potential to revolutionise communications, at least in the near field (the order of a few metres) for low power systems. In this paper, we consider the basic physics and some of the principle mathematical models associated with the development of this new disruptive technology in order to provide a guide to those engaged in current and future research, a fractal Graphene antenna being an example of an advanced material for demanding applications. This includes some example simulations on the THz field patterns generated by a fractal patch antenna composed of Graphene whose conductivity is taken to scale with the inverse of the frequency according to a 'Drude' model. The approach to generating THz sources using Graphene is also explored based on Infrared laser pumping to induce a THz photo-current.

1. Introduction

The theoretical principles of what is now known as Fractal Geometry can be traced back to the work of mathematician Gottfried Leibniz in the 17th century. The theoretical properties of Graphene were first explored in the late 1940s by Philip Wallace [1] as a starting point for

understanding the electronic properties of Graphite. Similarly, the design and implementation of radio antennas has been ongoing since the pioneering work of Heinrich Hertz [2] in the late 1880s following the theoretical prediction of Electromagnetic (EM) wave propagation by James Clark Maxwell in the 1860s. This paper investigates the coupling of fractal structures and the (electrical) properties of Graphene to design a new type of antenna operating in the THz region of the electromagnetic spectrum. The paper provides a contribution in the current quest to fill the 'THz gap' as illustrated in Figure 1, [4]. This gap is arguably the last of the frequency bands to be considered in the field of wireless communications. It is desirable to 'fill this gap' because communications system that operates at frequencies in the THz band will facilitate the wireless communication of binary information at a rate of Tera bits per second (Tbps), provided a suitable modulation method is available, which is not possible at lower frequency bands.

Technological solution to filling the THz gap represents a transition between the field of electronics for the generation of kHz, MHz and GHz radiation and the field of photonics in which binary information is transmitted through a sequence of laser light pulses in the optical frequency band $\sim 10^{15}$ Hz. The THz frequency band is therefore a band (the last band of it type) where it is physically possible to communicate using a wireless system. To realise this requires an antenna to be fabricated which is on the scale of the wavelength (i.e. the μm-nm scale) given that the physical size of an antenna generally reflects the wavelength at which the antenna radiates an electromagnetic field. For this reason, the power rating of such THz systems is relatively low, constraining the effective scale over which information can be communicated to the near field ($\sim$ meters). This is because there are no efficient methods to generate powerful emissions in the THz band at room temperature compared to lower and higher frequency sources as illustrated in Figure 2. It therefore becomes imperative to construct the antenna from a material that provides maximal current densities over the scale of the antenna. The current density is limited by the conductivity of the material and this is why Graphene is considered, i.e. it is the most conductive material known. Moreover, as shall be discussed in this paper, if the conductivity of Graphene is taken to scale with the inverse of the frequency (in the THz range), then the strength of the electric field emitted by such a conductor becomes independent of the frequency.

The application of Graphene enables wireless communication for nano-scale electronic devices but with a significant reduction in the emission energies. As de-localised electrons on the surface of Graphene (known as 'Graphon's') oscillate, they create an electromagnetic wave which is emitted from the surface of the Graphene. This is referred to as a Surface Plasmon Polariton (SPP) wave which is an electromagnetic wave that travel along a metal-dielectric interface and enables an antenna to operate at the lower end of the THz frequency spectrum with significantly greater efficiencies than are available with copper and other metal-based antennas, for example. Nano-antennas based on SPP waves enable the conversion of light from free-space into sub-wavelength volumes establishing a way of communication using free electron propagation within networks of nano-sized devices. This is impacting on many nano-applications, including biochemical sensors, reconfigurable meta-surfaces, compact optoelectronic devices and wireless nano-sensor networks (nano-networks). Due to its unique electronic properties, Graphene has been identified as a promising platform for building integrated active plasmonic nano-antennas for wavelengths in the mid-infrared range, i.e. 10 - 100 THz.

The electrical properties of (mono-layer) Graphene are such that a Fermionic or Dirac electron fluid [5] is present on the surface of the material. Such a fluid is a form of condensed matter that can be effectively described by the Dirac equations. Although the Dirac equations describe fermions, the quasi-particles present within Dirac matter can have variable statistics. By using infrared laser pumping (i.e. irradiating the electron fluid with a coherent oscillating electric field in the infrared spectrum) to generate a resonant wave pattern in the electron fluid, a Graphene ribbon can be tuned to operate as a THz resonator [6]. The output of this resonator is then coupled to a fractal Graphene patch antenna, thereby producing a THz radiator in the near field.

In this context, the basic principles associated with the design of a fractal Graphene antenna are as follows:

(i) Graphene can be used to generate a source of THz radiation;

(ii) Graphon's can propagate over a surface without incurring a significant number of collisions leading to a loss of energy and thus, the oscillation of Graphon's generate EM fields with relatively high energy densities for the scale of the antenna;

(iii) Fractal geometric shapes can generate EM fields with multiple bands due to the spatial frequency characteristics of self-affine structures.

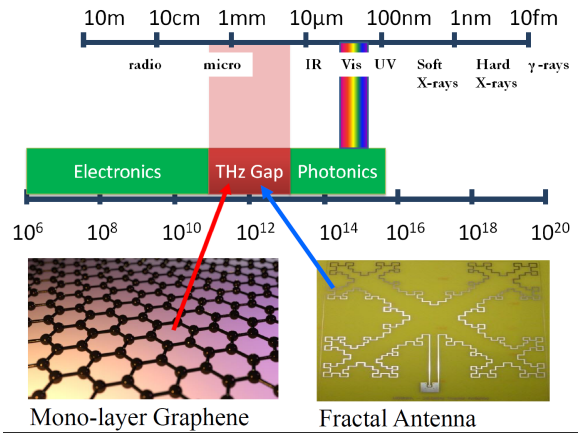

Figure 1. Illustration of the 'THz gap' and the role that Graphene and fractal antennas (composed from Graphene) can play in filling this gap.

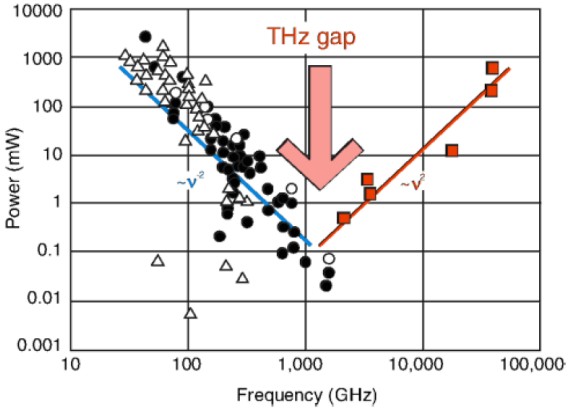

Figure 2. The 'THz gap' with respect to the output power and the frequency ν associated with different technologies: quantum cascade lasers (■), frequency multipliers (•), other electronic devices (△) and cryogenic sources (○) [4].

1.1. About this Paper

After a brief overview of electromagnetic theory and the electrical properties of Graphene, this paper presents some results of simulating the emission field patterns of a fractal Graphene antenna. The principal focus of the material presented is on THz wireless communications using nano-scale antennas. We consider the basic physical models that are the basis for the development of THz technology at this scale, models that include the far field emission of THz radiation and electron transport in Graphene. The combination of metallic structures and Graphene with gate-voltage dependent properties has already provided tuneable antennas with narrower frequency operations, e.g. [7] and [8]. In this paper, the aim is to design a compact structure while increasing the order of fractal structure to a high level by engineering nano-metric fractal Graphene. This fabrication can be achieved in practice using Electron Beam Lithography (EBL) or 3D nano-patterning using focused ion beam lithography, the Graphene being transferred on to a SiO_2 substrate to control the size and features at the nano-scale [9].

1.2. Structure of the Paper

The paper is structured in to the following sections.

- Section 2 provides a short overview and tutorial on the basic electromagnetic theory associated with antennas for harmonic frequency sources in order to introduce two basic antenna models for the intermediate and far fields which are used later in the paper.
- Section 3 uses the theory presented in Section 2 to introduce an idealised model for a fractal patch antenna and considers a new approach to quantifying the electric field generated by such an antenna in the far field based on the principles of scale invariant functions.
- Section 4 provides a short introduction to Graphene to contextualise Section 5, which focuses on the electrical conductivity of Graphene, in particular, its scaling relationship with frequency using a quantum mechanical model in different dimensions. The results show that the classical Drude model for the conductivity is only compatible with the quantum conductivity for a one-dimensional model.
- Section 6 presents some examples of a new Finite Element Analysis for a nano-metric scale fractal Graphene antenna.
- Section 7 discusses the physical principles associated with using a Graphene ribbon for generating a THz source and the optimal modulation method that should be applied.
- Sections 8, 9 and 10 present, respectively, a summary of the work, its principle conclusions and some future directions in regard to further development of the physical models considered, engineering issues and applications.

The principal original contributions are compounded in the material presented in Sections 3-7.

2. Physical Principles of EM Emissions from an Antenna

In this section we briefly review the physical models for the emission of EM radiation from an antenna focusing on a scalar model for a patch antenna. We begin with the basic electromagnetic equations for an antenna.

2.1. Basic Antenna Theory

For a three-dimensional continuum with a spatial vector $\mathbf{r}$ that is linear and isotropic, Maxwell's time t dependent equations (using the International System of units) can be written in the form

$$\nabla \cdot \epsilon \mathbf{E} = \rho \qquad \nabla \cdot \mu \mathbf{H} = 0$$
$$\nabla \times \mathbf{E} = -\mu \frac{\partial \mathbf{H}}{\partial t} \qquad \nabla \times \mathbf{H} = \epsilon \frac{\partial \mathbf{E}}{\partial t} + \mathbf{J}$$

where $\mathbf{E}(\mathbf{r}, t)$ is the electric field, $\mathbf{H}(\mathbf{r}, t)$ is the magnetic field, $\mathbf{J}(\mathbf{r}, t)$ is the current density, $\rho(\mathbf{r}, t)$ is the charge density, $\epsilon(\mathbf{r})$ is the permittivity and $\mu(\mathbf{r})$ is the permeability. The material parameters ϵ and μ can be written in the form $\epsilon = \epsilon_r \epsilon_0$ and $\mu = \mu_r \mu_0$ where $\epsilon_r \geq 1$ and $\mu_r \geq 1$ are the relative permittivity and relative permeability, respectively. In a perfect vacuum (where $\epsilon_r = 1$ and $\mu_r = 1$), $\epsilon = \epsilon_0 = 8.854 \times 10^{-12}$ Farads/meter and $\mu = \mu_0 = 4\pi \times 10^{-7}$ Henrys/meter. The equations above are the macroscopic form of Maxwell's equations for material properties characterised by ϵ and μ.

A conventional antenna is composed of conductive elements and can be considered to a 'conductive continuum' that is a good conductor in which a current (due to flow and oscillation of electrons) can be induced depending on the magnitude of an applied electric field and the conductivity σ (in Siemens/meter or S/m). The relationship between the electric field and the current density is given by Ohm's law, i.e.

$$\mathbf{J} = \sigma \mathbf{E} \tag{1}$$

Noting that $\nabla \cdot (\nabla \times \mathbf{H}) = 0$, for constant values of ϵ and σ,

$$\frac{\partial \rho}{\partial t} + \frac{\sigma}{\epsilon}\rho = 0$$

whose solution is

$$\rho(t) = \rho_0 \exp(-\sigma t/\epsilon),\ \rho_0 = \rho(t=0)$$

This result shows that the charge density decays exponentially with time. Thus, with values of $\epsilon \sim 10^{-12} - 10^{-10}$ Farads/meter, and, provided that σ is not a semi-conductor, the dissipation of charge is very rapid. For conductive materials, it is therefore physically reasonable to set the charge density to zero, and, for problems involving the radiation and/or interaction of electromagnetic waves with good conductors, we can consider the case when

$$\nabla \cdot \epsilon \mathbf{E} = 0 \tag{2}$$

This is a useful result as it allows a relatively simple scalar model to be developed for the emission of an electric field from an antenna (at least for the case when ϵ is taken to be a constant).

2.2. Model for a Scalar Wave Field
From Maxwell's equations given above, we can write

$$\nabla \times \nabla \times \mathbf{E} = -\mu \frac{\partial}{\partial t} \nabla \times \mathbf{H} = -\mu \frac{\partial}{\partial t} \left(\epsilon \frac{\partial \mathbf{E}}{\partial t} + \mathbf{J} \right) \text{ or } \nabla \times \nabla \times \mathbf{E} + \epsilon\mu \frac{\partial^2}{\partial t^2} \mathbf{E} = -\mu \frac{\partial}{\partial t} \mathbf{J}$$

Thus, noting that $\nabla \times \nabla \times \mathbf{E} = \nabla(\nabla \cdot \mathbf{E}) - \nabla^2 \mathbf{E}$, and, given Equation (2), for constant ϵ, we obtain a wave equation for the electric field with a wave velocity c given by

$$\nabla^2 \mathbf{E} - \frac{1}{c^2} \frac{\partial^2}{\partial t^2} \mathbf{E} = \mu \frac{\partial}{\partial t} \mathbf{J} \text{ where } c = \frac{1}{\sqrt{\epsilon\mu}}$$

In this case, the electric field is the same for any vector component of the current density. There is no field component coupling and we can therefore work with the scalar wave equation

$$\nabla^2 E - \frac{1}{c^2} \frac{\partial^2}{\partial t^2} E = \mu \frac{\partial}{\partial t} J \tag{3}$$

where E and J are any one of the three components of the corresponding vector fields. The interpretation of Equation (3) is that a rate of change in time of the current density J generates an electric wave field E. This is is a scalar antenna model. It is predicated on Equation (3) and consequently, does not take into account polarisation effects.

For a three-dimensional model of an antenna, the current density is of compact support $\mathbf{r} \in \mathbb{R}^3$. The electric field generated by a rate of change in the current density is taken to exit both inside and outside the domain $\mathbf{r} \in \mathbb{R}^3$. For $\mathbf{r} \notin \mathbb{R}^3$ where $\mathbf{J}(\mathbf{r}) = \mathbf{0}$ this electric field induces a magnetic field. Hence

$$\nabla \times \mathbf{H} = \epsilon \frac{\partial \mathbf{E}}{\partial t}$$

from which is follows (form Maxwell's equations) that the magnetic field $\mathbf{H}$ also adheres to a wave equation, i.e.

$$\nabla^2 \mathbf{H} - \frac{1}{c^2} \frac{\partial^2}{\partial t^2} \mathbf{H} = 0$$

Thus, a rate of change in current density induces an electric wave field which in turn induces a magnetic wave field. The combined fields generate an electromagnetic wave which is a self-propagating wave requiring no medium of support. This is because the oscillation of an electric field yields an oscillating magnetic field which in turn, generates another cycle of the electric field and so on, i.e. each electric and magnetic field component creates the other in a succession that leads to the propagation of an EM field in 'free space' where, for a vacuum

$$c_0 = \frac{1}{\sqrt{\epsilon_0 \mu_0}} \simeq 3 \times 10^8 \text{ ms}^{-1}, \;\; c \leq c_0$$

The 'arrival' of an EM field at some 'receiver' antenna with conductivity σ then induces a current density through the electric field component given by Equation (1).

2.3. Model for Harmonic Oscillation

From Equation (3), it is clear that to produce an electric field, the current density (the source function) can not be a constant but must undergo some change in time, the characteristic rate of change determining the characteristics of the electric field that is generated. Most antennas utilise a current density source that is oscillatory, in particular, simple harmonic oscillators. In this case we can consider the transformations $J := J\exp(-i\omega t)$ and $E := E\exp(-i\omega t)$ for angular frequency ω. With $\epsilon = \epsilon_0$ and $\mu = \mu_0$, Equation (3) can then be reduced to the inhomogeneous Helmholtz equation

$$(\nabla^2 + k^2)E(\mathbf{r}, k) = -ikz_0 J(\mathbf{r}) \tag{4}$$

where $k = \omega/c_0$ and $z_0 = \mu_0 c_0 \simeq 377$ Ohms is the impedance of free space. Note, that a transformation using $\exp(i\omega t)$ instead of $\exp(-i\omega t)$ is equally valid and only changes the polarity of the source term in Equation (4) and thus, the polarity of a solution to Equation (4).

The harmonic transformation to Equation (4) allows a solution to be formulated through application of the three-dimensional Green's function [10]. For homogenous boundary conditions, when $E = 0$ and $\nabla E = \mathbf{0}$ on the surface of J, this solution is given by [10]

$$E(\mathbf{r}, k) = ikz_0 \int\limits_{\mathbf{s}\in\mathbb{R}^3} \frac{\exp(ik \mid \mathbf{r} - \mathbf{s} \mid)}{4\pi \mid \mathbf{r} - \mathbf{s} \mid} J(\mathbf{s}) d^3\mathbf{s} \equiv ikz_0 \frac{\exp(ikr)}{4\pi r} \otimes J(\mathbf{r}) \tag{5}$$

where $\otimes$ denotes the (three-dimensional) convolution integral over the spatial domain of the current density which is of compact support, i.e. $J(\mathbf{r}) \; \exists \; \forall \; \mathbf{r} \in \mathbb{R}^3$.

Equation (5) provides a general solution for the electric field generated by a (current density) source. It can be appreciated physically by considering a complex of oscillating electrons undergoing a harmonic acceleration given that a free charged particle undergoing an acceleration radiates an EM field. A conductive material is composed of delocalised electrons which are relatively free to oscillate within the crystal lattice of the material. A single electron oscillating at frequency ω represents a (three-dimensional) point source $\delta^3(\mathbf{r})$ which radiates a field described by the Green's function itself, i.e.

$$g(\mathbf{r}, k) = \frac{\exp(ikr)}{4\pi r}, \; r \equiv \mid \mathbf{r} \mid \tag{6}$$

which is the solution of

$$(\nabla^2 + k^2)g(\mathbf{r}, k) = -\delta^3(\mathbf{r})$$

Thus, the field generated by a complex of oscillating electrons at different points in space (determined by the spatial extent of an antenna) is the sum of all such fields emanating from each

point. The sum must therefore be taken over the displaced fields according to the position of all such sources which is the reason why Equation (5) is characterised by a convolution integral. In this context, the current density, in particular, the source function ikz_0J, is that function which represents the spatial source of all such delocalised oscillating electrons in a conductive material as derived from Maxwell's macroscopic equations given in Section 2.1 subject to the condition that $\nabla \cdot \mathbf{E} = 0$. Note that, without this condition, we are required to solve the equation for the electric vector given by

$$\nabla \times \nabla \times \mathbf{E} - k^2\mathbf{E} = -ikz_0\mathbf{J}$$

which requires application of the Green's Dyadic. This model is considered later on in regard to the simulation of the electric field generated by a THz fractal Graphene antenna.

2.4. Intermediate and Far Field Solutions

Given Equation (5), our purpose is to generate an expression for the electric field E that is outside the spatial domain $\mathbf{r} \in \mathbb{R}^3$ of the current density J. There are two standard results that can be formulated in this respect. Both of these results come from applying an approximation to the convolution kernel - the Green's function - in Equation (5).

It is shown in Appendix A, that in the intermediate or Fresnel zone,

$$E(\mathbf{r}, k) = \frac{ikz_0}{4\pi r}\exp(ikr/2)\int\limits_{\mathbf{s}\in\mathbb{R}^3} \exp(i\alpha \mid \mathbf{r}-\mathbf{s} \mid^2)J(\mathbf{s})d^3\mathbf{s} = \frac{ikz_0}{4\pi r}\exp(ikr/2)K(\mathbf{r}, k)$$

where

$$K(\mathbf{r}, k) = \exp(i\alpha r^2) \otimes J(\mathbf{r}) \tag{7}$$

and $\alpha = k/2r,\ r \notin \mathbb{R}^3$ and in the far field,

$$E(\mathbf{r}, k) = \frac{ikz_0}{4\pi r}\exp(ikr)\widetilde{J}(\mathbf{k})$$

where, with $\mathcal{F}_3$ denoting the three-dimensional Fourier transform operator,

$$\widetilde{J}(\mathbf{k}) = \mathcal{F}_3[J(\mathbf{s})] = \int\limits_{\mathbf{s}\in\mathbb{R}^3} \exp(-i\mathbf{k}\cdot\mathbf{s})J(\mathbf{s})d^3\mathbf{s},\ \mathbf{k} = k\hat{\mathbf{n}},\ \hat{\mathbf{n}} = \frac{\mathbf{r}}{r} \tag{8}$$

The electric field in the intermediate zone is determined by a convolution integral - Equation (7) - and the electric field in the far zone is determined by a Fourier transform - Equation (8). Thus, in the far field, which is the more usual case in antenna theory, the power distribution of the electric field is given by

$$\mid E(\mathbf{r}, \omega) \mid^2 = \frac{k^2z_0^2}{16\pi^2r^2} \mid \mathcal{F}_3[J(\mathbf{r})] \mid^2 \sim 10^{-14}\frac{\omega^2}{r^2} \mid \mathcal{F}_3[J(\mathbf{r})] \mid^2$$

showing that the electric field intensity is limited by the inverse square law but varies as the square of the frequency.

The far field model for radiation emission from an antenna compounded in Equation (8) is the basic model used for analysing antenna designs in order to evaluate the spatial characteristics of the field pattern that they generate. There is a synergy between this model and the principles of Fourier optics where a well corrected and diffraction limited lens is taken to perform a Fourier transform in the focal plane. The Fourier transformation which takes place is of light that has been scattered from an object, the model for the far field scattering being given by the Fourier transform of the object. Although near field analysis of an antenna is possible through application of Equation (7), in most cases, we are interested in antennas that emit and receive an EM field that is some distance away from the source of emission. Hence, a far field analysis is most common.

2.5. Idealised Model for a Patch Antenna

A patch antenna is an antenna with a low profile, mounted on a flat surface. It typically consists of a flat rectangular sheet or 'patch' of conductive material (typically a metal), mounted on a larger dielectric substrate (with a relative permittivity ϵ_r of depth h and dimensions $L \times W$) as illustrated schematically in Figure 3. A second ground plate is then mounted on the same substrate below the patch which produces a resonance generated by what is in effect a micro-transmission line with a length of approximately one-half the wavelength of the EM wave to be radiated. The dielectric substrate must be a stable homogenous insulator, ideally, with as lower relative permittivity as possible. This is because the bandwidth is inversely proportional to relative permittivity [11]. In this context, Silicon Dioxide SiO_2 has and remains the most commonly used insulator. It is the primary gate dielectric material in metal-oxide-semiconductor field effect transistors, for example, and is used in the fabrication of many patch antennas.

If we consider the patch to be infinitely thin in the z-plane, then we can take a patch antenna to represent a source where the current density is given by $J(\mathbf{r})\delta(z),\ \mathbf{r} \in \mathbb{R}^2$. The effect of this is to reduce Equation (7) to the form,

$$K(\mathbf{r}) = \exp(i\alpha r^2) \otimes J(\mathbf{r}) \tag{9}$$

where $\otimes$ now denotes the two-dimensional convolution integral [ignoring scaling by the phase-only function $\exp(i\alpha z^2)$], and Equation (8) to

$$\widetilde{J}(\mathbf{k}) = \mathcal{F}_2[J(\mathbf{r})] \tag{10}$$

where $\mathcal{F}_2$ denotes the two-dimensional Fourier transform with spatial frequencies $k_x = kx/z$ and $k_y = ky/z$. Thus, for an infinitely thin patch antenna, the electric field pattern in the two-dimensional plane, far from the plane of the patch, is determined by the two-dimensional Fourier transform of the current density. Since x/z and y/z define the tangents in the x and y planes, respectively, it is common to visualise the electric field using a polar plot in which the electric field 'strength' (the power spectrum given by $\mid \widetilde{J}(\mathbf{k}) \mid^2$) is plotted as a function of the angle from the patch plane to the Fourier plane as illustrated in Figure 4. This provides a quasi-physical visualisation of the radiating field pattern which is typically viewed on a logarithmic scale in order to enhance the relative amplitudes of the higher frequency components of the pattern - the 'side-lobes'.

In the case of Figure 4, the field pattern is a colour coded surface representation of the field intensity and includes the current density distribution in the patch plane. This is typical of the graphical representations used to visualise both the current density and the electric field pattern compounded in Equation (10). If the electric field pattern $\widetilde{J}(kx/z, ky/z)$ for a given value of k is known at a distance z from the source, then the current density distribution induced at a receiver is taken to be given by (from Ohm's law) $J(x, y) = \sigma(x, y)\widetilde{J}(x, y),\ x := kx/z, y := ky/z$. This result does not of course take into account the scaling constant $\sim ikz_0/4\pi z$ associated with the electric field but it does provides a relationship between the electric far field pattern and the induced current density in terms of the two-dimensional conductivity function $\sigma(x, y)$ which defines the 'shape' of a receiver (infinitely thin patch antenna).

Given Equations (9) and (10) where $J = \sigma E$, it is clear that, for a fixed geometry, the greater the conductivity of the materials from which the antenna is made, the larger the amplitude of the electric field that is emitted. Similarly, for a given electric field amplitude at a distance z, the greater the conductivity of the receiving antenna, the higher the induced current density. Given that the electric field amplitude is proportional to the frequency, it is clear that making antennas from highly conductive materials operating at very high frequencies provides for greater electric field strengths and induced current densities. On the other hand, since the physical size of a patch antenna has to be of the order of the wavelength, operating at

higher frequencies requires a reduction in their physical size and therefore the power that can be applied - essentially the amplitude of the current density - subject to the conductivity of the material from which the antenna is composed. This leads to the application of Graphene as a suitable material or constructing high frequency antennas in the THz region because Graphene is the most conductive of any room temperature material currently known. While the precise definitions and experimental determinations very, its conductivity is the order of 10^8 S/m which is an order of magnitude greater than the most highly conductive of the elements such a Copper, Silver and Gold, for example, from which conventional antennas are composed - primarily pure copper and copper based amalgam's due to the price of copper being lower.

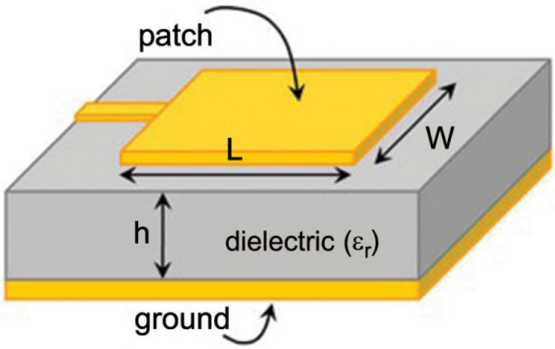

Figure 3. Example of a patch antenna.

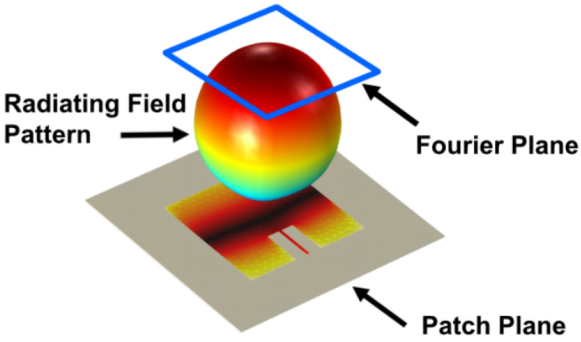

Figure 4. Example visualization of the radiating electric field patterns generated by a patch antenna.

3. Fractal Patch Antennas

A fractal is a self-similar or self-affine function that may be deterministic or stochastic (a statistically self-affine field); it is a field that looks the same or similar at different scales and maybe exactly self-similar at different scales or have an affinity at different scales [12]. In either case, fractals are objects that have a specific fractal dimension, a value that is strictly greater than the topological dimension upon which the fractal is based. Thus, a fractal curve is one with a fractal dimension $D \in (1, 2)$ and a fractal surface has a fractal dimension $D \in (2, 3)$ and so on. As a fractal dimension approaches the upper bound, it becomes more 'space filling' and the 'texture' of the object exhibits greater 'complexity'. This is why the fractal dimension of a field can be used to classify texture which is an otherwise rather elusive term. However, the fractal dimension alone is not a unique measure as different fractals that exhibit different textures can have the same fractal dimension. In this section, we provide a short study of the effect on introducing patch antennas with a fractal structure.

3.1. Scale Invariant Functions and the Characteristic Scaling Properties of Fractals

For some scaling factor L, say, a scale invariant function $f(\mathbf{r})$, $\mathbf{r} \in \mathbb{R}^n$ is one that conforms to the equation

$$L^q f(\mathbf{r}) = f(L\mathbf{r}),\ q > 0 \tag{11}$$

for some choice of exponent q and for any dilation L. A fractal is usually scale invariant but only for a discrete set of values L with translations and rotations often being required to match the fractal with itself at different (discrete) scales. An exact self-similar fractal is one for which $q = 1$.

Deterministic fractals are mostly based on iterative sequences that produce a consecutive repetition of an original object - its shape - to provide a number of scaled down copies of itself.

If, at each iteration, the scale length of an object is reduced by a factor L, and, at each iteration N, copies of the object are made and re-assembled in a coordinated way that is the same at each iteration, then the resulting pattern can be taken to adhere to the equation $NL^D = 1$. The fractal dimension is then given by

$$D = -\frac{\log(N)}{\log(L)} \tag{12}$$

Figure 5 provides an example of this iterative process to produce what is known as a Cantor set. In this case, starting at the top the graphic, we consider a line of length 1 unit. The line is cut into three lines of equal length, one of which is discarded (in the case of Figure 5, this is the central line but it could be the lines to the left or right hand side). If this process is then repeated again and again, then at each iteration, it is clear that $N = 2$ and $L = 1/3$ from which is follows that $D = \log(2)/\log(3) \simeq 0.6309$, i.e. $D \in (0, 1)$. The Cantor set is an example of so called 'fractal dust'. This is because it has a fractal dimension that is less than a topological dimension of 1. Note, that if the line at each iteration is retained instead of deleted, then at each iteration $D = \log(3)/\log(3) = 1$ and the original topological dimension is retained. This is why fractals are referred to as space filling objects as $D \to n$ for a topological dimension $n = 1, 2, 3$.

An important relationship between q, n and D is given by [12]

$$D = \frac{3}{2}n + 1 - q$$

where the range of the values of q is strictly determined by the value of n and the corresponding range of values of D, i.e. $n = 0 \Rightarrow D \in (0, 1)$, $n = 1 \Rightarrow D \in (1, 2)$, ... This relationship applies, for example, to the scaling characteristics associated with the amplitude spectrum $F(\mathbf{k})$ of a fractal $f(\mathbf{r})$ given by [12]

$$F(\mathbf{k}) \sim \frac{1}{\mid \mathbf{k} \mid^q},\ q > 0 \tag{13}$$

Ignoring scaling coefficients, the fractal then has a scaling relationship characterised by by $1/\mid \mathbf{r} \mid^{n-q},\ n - q > 0,\ \mathbf{r} \in \mathbb{R}^n$ so that for some object function $o(\mathbf{r})$, say,

$$f(\mathbf{r}) = o(\mathbf{r}) \otimes \frac{1}{\mid \mathbf{r} \mid^{n-q}}$$

where the fractal is taken to conform to a linear stationary process, i.e. the sum of all points over which the object function is constructed subject to the scaling property $1/\mid \mathbf{r} \mid^{n-q}$. This is a fundamental 'signature' of a self-affine function, given that

$$f(L\mathbf{r}) = \int_{-\infty}^{\infty} \frac{o(\mathbf{s})}{\mid L\mathbf{r} - \mathbf{s} \mid^{n-q}} d^n\mathbf{s} = L^n \int_{-\infty}^{\infty} \frac{o(L\mathbf{s})}{\mid L\mathbf{r} - L\mathbf{s} \mid^{n-q}} d^n\mathbf{s} = L^q f(\mathbf{r})$$

which recovers Equation (11).

3.2. Why use a Fractal Patch Antenna?

A conventional patch antenna (modeled as a thin and primarily rectangular conductor) has a topological dimension of $n = 2$. The wavelength of the emission/reception is essentially on the same physical scale of the patch. For communications in the GHz or microwave range, this is on the scale of a few centimeters. A wire antenna (with same same electrical conductivity as the patch antenna) with a topological dimension of $n = 1$ and of the same scale will also radiate and EM field but with significant less energy. This is due to the following:

(i) the population density of delocalised electrons is lower;

Figure 5. The Cantor Set with a Fractal Dimension of 0.6309.

(ii) it is not possible to develop a 'line resonator' to produce a comparable power output.

Thus, the first point to note about a fractal patch antenna where $D \in (1, 2)$ is that the energy of an emission will be less; there is, by the very nature of a 'fractal patch', less conductive material to source an electric field. On the other hand, the self-affine structure of a fractal antenna provides, what is in effect, a set of multiple antennas in one, supporting a multitude of frequency bands. To explain this, we refer to Figure 6. This figure shows a Sierpinski and a Tree antenna fabricated from copper. In the former case, the figure illustrates the correlation between the physical size of the Sierpinski triangle and it relationship to a single wavelength of an electric field (emitted or received) and how electric wave fields consisting of $2, 4, 8, 16$ and 36 periods (from left to right of the central graphic) relate to the size of the 'triangles' from which this self-similar structure is composed. The Sierpinski triangle is a deterministic fractal obtained by iteratively replicating an equilateral triangle four times at half the scale length of the original and deleting one of the four resulting triangles (the central component) to leave just three. Hence, at each iteration $N = 3$ and $L = 1/2$, giving a fractal dimension of $D = \log(3)/\log 2 \simeq 1.5850$.

There are a multitude of fractals that can, in principle, be used as patch antennas but, strictly speaking, for them to be patch antennas necessitates the use of fractals such that $D \in (1, 2)$. On the other hand, it is possible to fabricate patch antennas of the type shown in Figure 5 for $D \in (0, 1)$ but only when the current density is taken to exist in the background space to the fractal structure. This is because a continuous current density is required within and over the extent of the antenna. Thus, in the case of Figure 5, the Cantor set describes the 'geometry' of the dielectric substrate upon which the conductor is mounted and not the conductor itself.

In regard to patch antennas for which $D \in (1, 2)$, the choice of which components of the pattern are used to support a current density depends critically on the continuity of the structure so that electrons can oscillate and flow continuously over the fractal structure as a whole. This leads to some important issues that need to be considered in the practical fabrication of such antennas which include:

(i) the number of iterations that can be applied in practice given the material from which the antenna is made, i.e. what are the engineering limits associated with cutting a material into a fractal patch antenna at a specific physical scale?

(ii) the extent to which the fine structure elements of the fractal antenna do not over heat and/or possibly melt for the current densities that are applied.

Points (i) and (ii) are interrelated because in order to maximise the number of multiple bands that a fractal antenna can operate over, the structure must be as fine as possible. However, to optimise the power output from such an antenna, it must be fabricated from a highly conductive material with minimal resistance to the flow and oscillation of electrons, thereby allowing a relatively high current density to be applied which does not lead to over heating and/or burn-out of the fine structure components. These issues lead naturally to the application of Graphene

to fabricate such antennas using technologies that are available to cut a Graphene mono-layer to produce a fractal structure using e-beam lithography, for example.

Irrespective of the (conductive) material that is used to fabricate a fractal antenna, such an antenna provides, multi-band support, wide bandwidths and high gains at smaller dimensions. The dimensions of such antennas becomes critical in regard to generating THz emissions since the wavelength of an emitting and receiving antenna is determined by its physical size; the smaller the wavelength, the smaller the antenna. In this context, the fine structure at small scales required to fabricate a THz fractal patch antenna necessitates the use Graphene since it is the most conductive of all known (room temperature) materials.

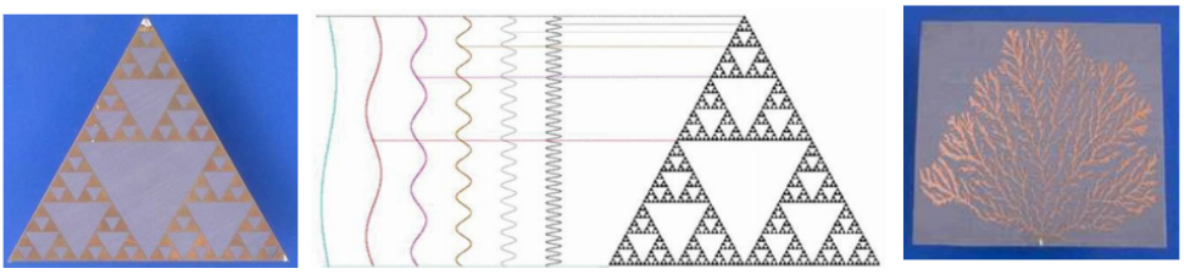

Figure 6. A deterministic Sierpinski triangle antenna (left), a schematic explanation of its multi-band properties (centre) and a further example of a random fractal 'tree' antenna (right).

3.3. Far-Field Patterns Generated by Fractal Patch Antennas

In the far field (specifically the Fourier plane that is parallel to the patch plane), the electric field pattern generated by a patch antenna is characterised by Equation (10), namely, the two-dimensional Fourier transform of the (two-dimensional) current density. It is therefore informative to study the Fourier transform of 'patch fractals' for $D \in (1, 2)$.

Figure 7 shows the radiation far-field patterns (specifically, the logarithmic power spectrum - $\log \mid \widetilde{J}(\mathbf{k}) \mid^2$ - for three patches with a topological dimension of 2 and fractal dimensions of 1.8928 (a Sierpinski Carpet) and 1.5850 (a Sierpinski Triangle). In these examples, it is clear that the power spectra of the fractal structures is broader than the power spectrum associated with a continuous square patch when the (amplitude) spectrum is characterised by a separable sinc function.

Since the power spectrum of a fractal is characterised by the scaling relationship given by Equation (13), for a fractal patch antenna, the log power spectrum is characterised by

$$\log P(\mathbf{k}) = \log \mid F(\mathbf{k}) \mid^2 \sim (2D - 5) \log \mid k \mid, \; D \in (1, 2)$$

Thus as $D \to 2$ the power spectrum is proportionately greater over the equivalent range of $\log \mid k \mid$ indicating that greater power will be emitted by a fractal patch antenna for higher values of the fractal dimension. However, as discussed in the latter part of the previous subsection, this requirement has to take into account the engineering associated with fabricating high fractal dimension fractals, especially those that are to be composed of mono-layer Graphene.

The far-field radiation pattern generated by a fractal patch antenna can be quantified theoretically by analysing the Fourier transformation of a scale invariant function. On the basis of Equation (10), we consider the geometry of the current density of the antenna to be characterised by the equation

$$L^q J(\mathbf{r}) = J(L\mathbf{r}), \; \mathbf{r} \in \mathbb{R}^2, \; q = \frac{5}{2} - D, \; D \in (1, 2)$$

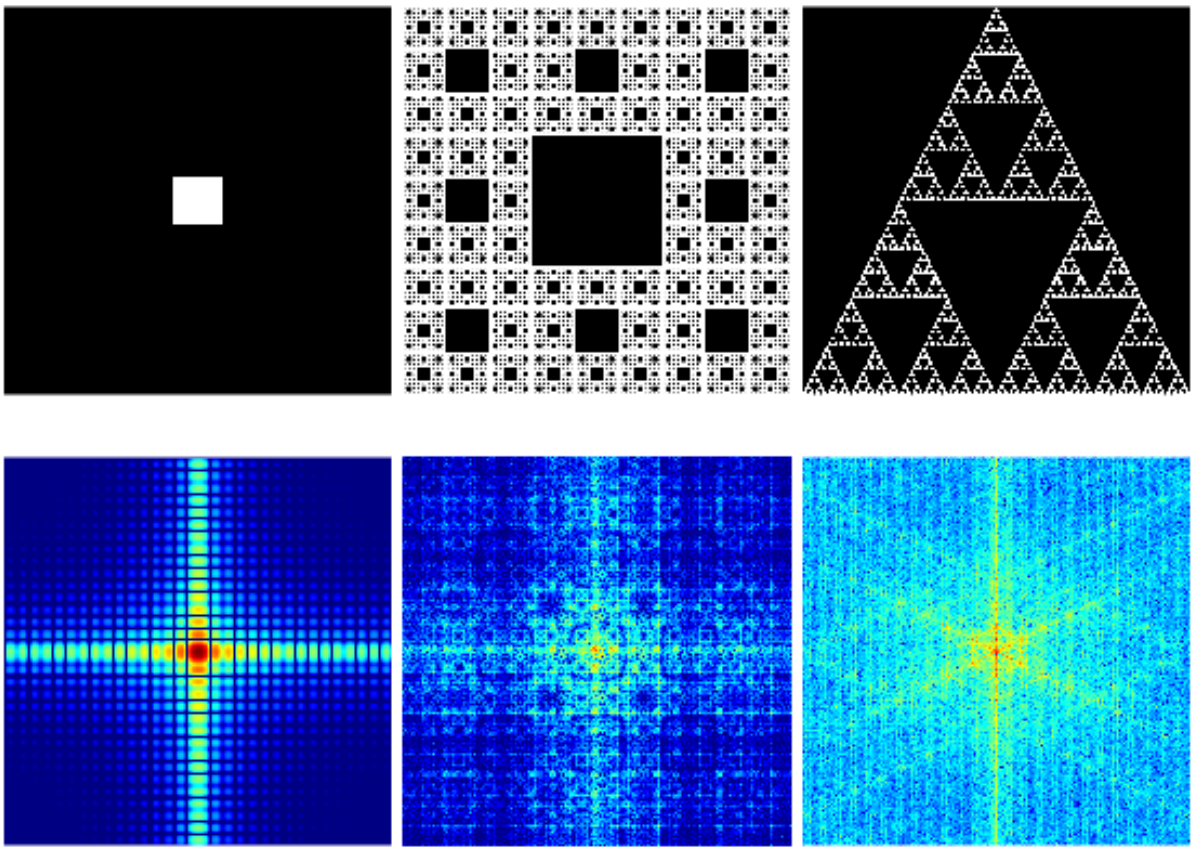

Figure 7. From left to right: Colour coded displays (using the MATLAB 'jet' colour map) of the power spectra (below) plotted on a logarithmic scale for (above) a conventional patch antenna (with a topological dimension of 2), a Sierpinski Carpet ($D = 1.8928$) and a Sierpinski Triangle ($D = 1.5850$).

The electric field is therefore characterized by

$$L^q \widetilde{J}(\mathbf{k}) = L^q \mathcal{F}_2[J(\mathbf{r})] = \mathcal{F}_2[J(L\mathbf{r})]$$

and using the scaling theorem for a two-dimensional Fourier transform, i.e.

$$\mathcal{F}_2[J(L\mathbf{r})] = \frac{1}{L^2}\widetilde{J}\left(\frac{\mathbf{k}}{L}\right)$$

we have

$$L^{2+q}\widetilde{J}(\mathbf{k}) = \widetilde{J}\left(\frac{\mathbf{k}}{L}\right)$$

showing that the electric field is a inverse scaled invariant function, i.e. with $L := 1/L$,

$$\frac{1}{L^{2+q}}\widetilde{J}(\mathbf{k}) = \widetilde{J}\left(L\mathbf{k}\right) \text{ or } L^q\widetilde{J}(\mathbf{k}) = L^{2(1+q)}\widetilde{J}\left(L\mathbf{k}\right)$$

This means that the electric field generated by a fractal patch antenna is itself a re-scaled scale invariant function.

There is an interesting issue in regarding to this result, which is to consider what fractals have the same form in Fourier space. This is similar to the problem associated with conventional functions, namely, classifying those functions that are self-characteristic under Fourier transformation. Although not clearly evident from Figure 7 due to the limited resolution of the image, the Sierpinski triangle is one such fractal whose basic structure appears to be 'reproduce' in Fourier space. Whether this is unique to Sierpinski triangle or otherwise is the subject of further investigation and lies beyond the scope of this publication.

Figure 7 is illustrative of a feature of fractal antennas which is that their side lobe emission (i.e. the power output at wide angles) is significant compared to a square patch antenna. This means that such antennas are not directional which is a potential weakness for long range communications. However, given that in the THz range, such antennas are taken to be operable in the near field, this issue is not so relevant.

4. Introduction to Graphene

Graphene, specifically mono-layer Graphene, consists of a single layer of carbon atoms arranged into a two-dimensional hexagonal-based honeycomb lattice and can be considered as a basic building block for all Graphitic materials of other dimensions [13]. First discovered in 2004 at the University of Manchester [14], it is currently the only known two-dimensional (one-atom-thick) crystalline form of matter [15]. Each cell of the lattice has a delocalised electron cloud above and below the plane. This allows electrons that are introduced to the plane of the lattice to 'skate' freely over the surface with minimal resistance. Thus, electron transport measurements show that Graphene has a remarkably high electron mobility at room temperature, with reported experimental values in excess of $200,000$ $\mathrm{cm^2V^{-1}s^{-1}}$ at electron densities of $2 \times 10^{11}\mathrm{cm^{-2}}$ [16] with a conductivity of $\sim 10^8$ S/m.

Graphene is a semi-metal (a zero-gap semi-conductor) with a wide range of potential applications including ballistic transistors, nano-ribbons, ultra-sensitive molecular sensing, super capacitance and Spintronics. Its application to constructing fractal Graphene antennas is a direct result of its conductivity in which electrons can flow and oscillate with out the intrinsic resistance that occurs in other materials, thereby providing EM fields with relatively greater energy densities, given the fine structure of the fractal that is required (to produce of multiple frequency channels) and the physical size of a fractal antenna necessary to operate in the THz range.

On a theoretical basis at least, two-dimensional Graphite has been studied since the late 1940s and is widely used for describing properties of various carbon-based materials. An interesting property of Graphene is that the charge carriers are relativistic. Even though they are not actually traveling at relativistic speeds, their structural interaction causes them to act like two-dimensional Dirac Fermions with zero rest mass at the Dirac points on the six comers of the hexagon although this pseudo-relativistic description is restricted to the chiral limit. Fermions are (relativistic) particles that are described by a Spinor field and electrons are taken to have a spin of $1/2$. Thus, the charge carriers in Graphene have a unique property in that they mimic relativistic particles as described by the Dirac equation rather than the Schrödinger equation [17]. The relativistic-like description of electron waves on honeycomb lattices has been considered on a theoretical basis for many years and is now being applied in an attempt to understand the electronic properties of Graphene since the experimental discovery of the material [18], [19].

To understand why this is the case let us consider a particle based explanation. As is well known, a Carbon atom has four electrons that are 'free' to pair-bond with the outer most electrons of other molecules, including other carbon-based molecules. This is why Carbon can be used to produce long chain molecules. In (mono-layer) Graphene, each Carbon atom is electron pair bonded to three other Carbon atoms and not four. Thus, each Carbon atom in Graphene has one 'free' or 'delocalised' electron, and, since each hexagonal cell of the lattice

consists of six Carbon atoms, we can associate a total is six delocalised electrons with each cell, three of which lie below the plane of the Graphene and another three above the plane. In either plane, we can imagine three electrons (visualised as particles) 'rotating' around the (hexagonal) cell in their 'failed attempt' to pair-bond with another electron. Coupled with the fact that each of the three electrons repels the other, and, that this repulsion includes the electrons in all of the six neighbouring cells, the free electron in each cell continue to 'rotate' at a faster and faster rate obtaining a velocity of the order of 70% the speed of light. This is why the (free) electrons in Graphene are taken to be (near) relativistic particles. However, as always in quantum mechanics, a particle model is not a statement of reality but a liability of fantasy and we are required to visualise the electrons in the plane of a Graphene cell as an electron Cloud as illustrated in Figure 8.

If we consider the combined effect of all the electron clouds for each hexagonal cell in Graphene to be a continuum, then we can consider the planes above and below the Graphene to be composed of an electron fluid, specifically a Dirac or Fermionic fluid (due to the near relativistic speeds of the electrons in the fluid). Like other fluids, this electron fluid can support waves if it is 'pumped' by an external source. If the frequency of this pump is compatible with the physical extent of the Graphene surface (a Graphene ribbon with a finite length and width) then, in principle, it is possible to generate a resonance effect. This is discussed later on in this work in regard to using Graphene to generate THz radiation.

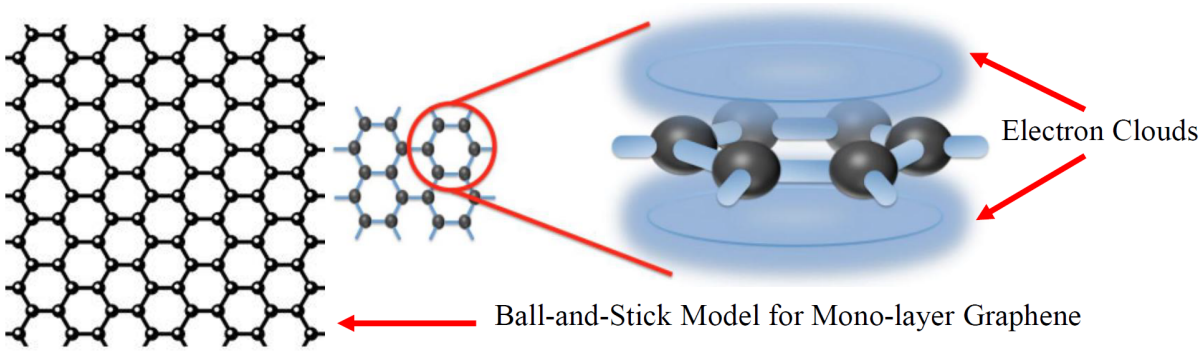

Figure 8. Schematic illustration of the electron clouds (each consisting of three electrons) that exist above a below the plane of mono-layer Graphene.

5. Conductivity of Graphene

While the theoretical 'relativistic properties' of Graphene remains to be fully correlated with experimental evidence, the non-relativistic properties of the material remain a subject of research in terms of (non-relativistic) incident electrons scattering from a two-dimensional electrostatic lattice composed of a regular sequence of localised potentials. These potential are derived from the delocalised electrons associated with the hexagonal nature of the primary structure of Graphene and are replicated throughout the lattice. The delocalised electron cloud represent a repulsive electrostatic potential with respect to any (free) electron propagating over the surface of the material due to the application of an electric field between a source and a drain. These free electrons weakly interact with each delocalised electron cloud scattering from the cloud. This is an effect which ultimately limits the conductivity of Graphene and introduces a frequency dependence.

The electrical conductivity of a material depends on how free the electrons are able to move through the lattice of the material. On the basis of this concept, it is clear that the greater the

electron Scattering Cross Section (SCS) is, the lower the conductivity will become. Developing accurate conductivity models for Graphene is a continuing field of research and, to date, there appears to no generalised all frequency model available. However, this is the case with many other materials, especially semi-conductors and meta-materials, for example. Nevertheless, a specific model for the conductivity of the material is crucial in the design and simulation of a Graphene based antenna, fractal or otherwise. This is because, given Equation (4), the source term is frequency dependent as is the current density itself if the conductivity of the material is also frequency dependent when $J = \sigma(\omega)E$. Thus, the purpose of this section if to briefly review the basis for developing models for the conductivity of Graphene in order to assess the frequency dependence of the source term in Equation (4).

5.1. Drude Model

The Drude model is a generic model for the conductivity of a material [20], [21]. For a time independent electric field with angular frequency ω_0, the model is compounded in the result

$$\sigma(\omega) = \frac{\sigma_0}{1 - i\omega\tau}$$

where τ is the mean free time between collisions (the 'relaxation time') with the delocalised electrons of the material and $\sigma_0 = ne^2\tau/m$ is the equivalent conduction of a direct current conforming to Ohm's law, e, n and m being the electron charge, electron number density and electron mass, respectively. For high frequencies, when $\omega\tau >> 1$, $\sigma \sim i\sigma_0/\omega\tau = ine^2/m\omega$. In this case, Equation (4) is reduced to the form

$$(\nabla^2 + k^2)E = -J \tag{14}$$

where $J = \mu_0 ne^2 E/m \sim 3.5 \times 10^{-14} nE$. The electron number density of Graphene varies quadratically with temperature but at room temperature (= 300 ^{o}K), $n \simeq 8.5 \times 10^{14}$ m^{-2} [22] and thus, $J \simeq 30.45E$.

Compared with Equation (4), the source term in Equation (14) is frequency independent so that the efficiency of the antenna remains the same for any frequency. This is important for a fractal antenna that, through its geometric configuration, can support many different frequency bands. It means that the limit of the number of bands for which the antenna is designed is limited only by the fine structure of the fractal that can be fabricated in practice and not by a reduction in the conductivity of the material with the frequency of the band. This result is predicated on the conductivity being inversely proportional to the frequency in the high frequency limit; ideally applicable in the THz range.

More advanced models for the (surface) conductivity of mono-layer Graphene have been considered in [23], for example. In this case, a Drude-type approximation for σ is obtained that is valid for mid-infrared wavelengths, where the intra-band conductivity term (due to transformations within electronic states) usually dominates over the inter-band term (describing the transformation between electronic bands, specifically from valence to conduction bands). An approximation for σ in the range 0.01-100 THz is then given by

$$\sigma \simeq \frac{e^2\mu_c\tau}{\pi\hbar^2(1 - i\omega\tau)} \sim \frac{i\sigma_0}{\omega},\ \omega\tau >> 1;\ \ \sigma_0 = \frac{e^2\mu_c}{\pi\hbar^2}$$

where μ_c is the carrier mobility $\sim 2\times10^3$ and $\hbar$ is the Dirac constant. In this case, the relaxation time is given by

$$\tau = \frac{\mu_c\mu_f}{ev_f^2}$$

where μ_f is the Fermi energy (the Chemical Potential) and v_f is the Fermi velocity of Dirac fermions in Graphene ranging from $8.5 \times 10^5 - 3 \times 10^6$ ms^{-1}.

5.2. Quantum Mechanical Models

One important assumption associated with the Drude model is that the electrons move in straight lines between (multiple) collisions. This is known as the free electron approximation and is equivalent to applying a point scattering model for electrons in the context of the quantum theory of conductivity. In this case, the conductivity is taken to be a macroscopic property of the SCS of electrons as they flow through the material. As the population density of scattering sites decreases, one can expect the back-scattering component associated with the SCS to decrease, which is analogous to the mean free time becoming larger, thereby producing a higher conductivity. In this context, if the forward-scattering component of the SCS is large and the back-scattering component is low, then the material will be a good conductor. For electron-electron interactions, the scattering cross-section is determined by the scattered wave function, in particular, the square modulus of the scattered wave function.

For $\mathbf{r} \in \mathbb{R}^n \mapsto V(\mathbf{r})$, the wave function $\psi(\mathbf{r}, k)$ of an electron (for the non-relativistic case) can be taken to conform to Schrödinger's equation, given by

$$(\nabla^2 + k^2)\psi(\mathbf{r}, k) = V(\mathbf{r})\psi(\mathbf{r}, k) \tag{15}$$

where $k^2 = 2m\omega/\hbar = 2mE/\hbar^2$, $E = \hbar\omega$ is the electron energy (for a wave function with angular frequency ω where $\hbar \simeq 1.054571817 \times 10^{34}$ Js is the Dirac constant) and $V(\mathbf{r}) := 2mV(\mathbf{r})/\hbar^2$ is the quantum scattering function; an asymptotic potential where $V(\mathbf{r}) \to 0,\ r \to 0$.

Consider a solution for $\psi(\mathbf{r}, k)$ which is given by the sum of an incident ψ_i and a scattered ψ_s fields, i.e.

$$\psi(\mathbf{r}, k) = \psi_i(\mathbf{r}, k) + \psi_s(\mathbf{r}, k) \text{ where } \frac{\|\psi_s(\mathbf{r}, k)\|}{\|\psi_i(\mathbf{r}, k)\|} << 1,\ \|\psi\| \equiv \left(\int \mid \psi(\mathbf{r}, k) \mid^2 d^n\mathbf{r} \right)^{\frac{1}{2}}$$

If we consider the incident field to be a unit amplitude plane wave given by $\psi_i(\mathbf{r}, k) = \exp(ik\hat{\mathbf{n}}_i \cdot \mathbf{r})$ where $\hat{\mathbf{n}}_i$ is a unit vector which points in the direction of the incident field, then Equation (15) has the approximate form

$$(\nabla^2 + k^2)\psi_s(\mathbf{r}, k) = V(\mathbf{r})\psi_i(\mathbf{r}, k) \tag{16}$$

This is known as the Born or weak scattering approximation and assumes that multiple scattering effects are negligible. This requires that $\|V(\mathbf{r})\| << 1$, i.e. $V(\mathbf{r})$ is a 'weak scattering potential'. The intensity of the wave function $\mid \psi_s \mid^2$ is the SCS.

The general solution (i.e. the Green's function transformation) to Equation (16) for the scattered field is [10]

$$\psi_s(\mathbf{r}, k) = -g(r, k) \otimes [V(\mathbf{r})\psi_i(\mathbf{r}, k)] \tag{17}$$

where $\otimes$ denotes the convolution integral over $\mathbf{r} \in \mathbb{R}^n$ and $g(r, k)$ is the free space Green's function given by the solution to

$$(\nabla^2 + k^2)g(\mathbf{r}, k) = -\delta^n(\mathbf{r})$$

The Probabilistic Current Density (PCD), which is the quantum equivalent to the current density associated with an electric field, is given by

$$\mathbf{J} = \frac{\hbar}{2im}[\psi^*(\mathbf{r}, k)\nabla\psi(\mathbf{r}, k) - \psi(\mathbf{r}, k)\nabla\psi^*(\mathbf{r}, k)]$$

and with $\psi = \phi \exp(iS/\hbar)$, where ϕ and S are real functions of $\mathbf{r}$ and k, we can reduce this expression for the PCD to the form

$$\mathbf{J} = \mid \psi \mid^2 \frac{\nabla S}{m}$$

This result provides a quantum equivalence to Ohm's law in the electromagnetic context where ∇S and $\mid \psi \mid^2$ are equivalent to an electric field and the conductivity, respectively. In this context, $\mid \psi \mid^2$ characterises the Quantum Conductivity (QC) which depends on the scattering potential coupled with the topological dimension over which ψ is evaluated.

Integrating over $\mathbf{r} \in \mathbb{R}^n$, we note that

$$\|\psi\|^2 \leq \|\psi_i\|^2 + \|\psi_s\|^2$$

It is then clear that for the same incident wave (representing an electron introduced into the material from a source, i.e. the value of $\|\psi_i\|^2$) the QC is determined by the SCS alone. We therefore now consider the calculation of of the SCS for $\mathbf{r} \in \mathbb{R}^n$ to derive frequency scaling relationships associated with the QC. The key to this is the functional form of the free space Green's functions that, in addition to the Green's function for $n = 3$ given by Equation (6) as discussed in Section 2.3, for $n = 1$ and $n = 2$ are given by [10]

$$g(x,k) = \frac{i}{2k}\exp(ikx) \text{ and } g(r,k) = \frac{\exp(i\pi/4)\exp(ikr)}{\sqrt{8\pi kr}},\ kr >> 1$$

respectively. Under the weak scattering approximation, Appendix B derives expressions for the QC using a Coulomb scattering potential. In so doing, we provide scaling relationships between the quantum conductivity and the frequency for $n = 1, 2, 3$.

5.3. Analysis of Results

On the basis of the results derived in Appendix B, it is clear the QC scales with the frequency according to $1/\omega^\alpha,\ \omega > 0$ where, depending on the dimension of the model that is applied $\alpha = 1,\ 1.5,\ 2$ for $n = 1,\ 2,\ 3$, respectively. In this context, the classical Drude model becomes compatible with a one-dimension quantum scattering model, and, on this basis, we can consider Equation (14) to be a model for the electric field generated by a Graphene antenna, whose source term is frequency independent. The application of a Coulomb potential assumes that electron-electron interactions are isolated and further consideration is necessary in regard to what type of (effective) potential an electron encounters when it is incident on a three component electron cloud such as exists in the local vicinity of a Graphene cell.

5.4. Bulk Conductivity

The bulk conductivity is related to the surface conductivity by $\sigma := \sigma/\Delta$, where Δ is the thickness of the Graphene layer which is taken to be much smaller than the excitation wavelength. In this way, Graphene can be modelled as a very thin ($\sim$ nm) three-dimensional material. For a Graphene sheet with relative permittivity ϵ_r, we can write the following equation for the (three-dimensional) electric field

$$(\nabla^2 + k^2\epsilon)E(\mathbf{r},k) = 0,\ \epsilon = \epsilon_r + i\epsilon_i \tag{18}$$

where $\epsilon_i = \sigma/(\epsilon_0\omega\Delta)$ and σ is the surface conductivity (taken to adhere to a Drude model).

The volumetric permittivity, ϵ, is assumed to be that of a Graphene layer with a finite thickness Δ which depends on the surface conductivity. The electric field is then determined primarily by the two-dimensional geometry of the (patch) antenna. In the context of Equation (18), the complex permittivity and the electric field are three dimensional entities. However, for a mono-layer Graphene patch of thickness Δ, only the surface conductivity is relevant, the permittivity over the thickness of the patch being taken to be given by ϵ_r alone. In either case, we can consider the value of ϵ_r to be that of Graphite, when $\epsilon_r \simeq 2.5$. Thus, for

three dimensional Graphene models ϵ is anisotropic with out-of-plane and in-plane components ϵ_r and $\epsilon_r + i\epsilon_i$, respectively.

As discussed earlier in this work, Equation (4) is a wave equation for the scalar electric field under the condition $\nabla \cdot \mathbf{E} = 0$. The equivalent equation to Equation (4) for a vector electric field is

$$\nabla \times \nabla \times \mathbf{E}(\mathbf{r}, k) - k^2 \epsilon \mathbf{E}(\mathbf{r}, k) = 0 \tag{19}$$

where we can write ϵ in terms of a complex refractive index with real and imaginary components n and κ, respectively, as $\epsilon = (n + i\kappa)^2$. In the case of Graphene, experimental measurements of n and κ are available in the region 0.15-0.95 μm which depends on the Graphene thickness and the substrate upon which it is mounted [28]. This is the basis for the simulations that are discussed in the following section.

6. Simulations

Simulations are performed for a Sierpinski triangle monopole antenna of nano-metric dimensions. This basic configuration is as follows:

- The Graphene fractal triangle has lateral dimensions of 640nm × 560nm and a thickness of 3nm;
- the smallest triangle from which the fractal is composed has lateral dimensions that are 1/16 times the 'fundamental triangle';
- the fractal triangle is deposited on top of a 10nm SiO_2 substrate which rests on top of a 10nm thick Si substrate;
- the fractal antenna is fed by a coaxial cable and placed on a ground plane which has a diameter of 800nm and a thickness of 25nm.

Macro-scale Sierpinski triangle monopole antennas of this type are intended to be used for different discrete frequency bands. Nano-scale equivalent antennas are not expected to operate in the same way as the materials have their own properties and cannot be assimilated to be a Perfect Electric Conductor (PEC). At the nano-scale, the volumetric conductivity is described in terms of the real and imaginary components of the relative permittivity, which can be expressed in terms of the components of the (complex) refractive index.

We study a Sierpinski triangle monopole antenna made of Gold, Graphene and Silicon by solving Equation (19) for a complex refractive index in the frequency domain over the range 10-700 THz [29]. A few layers of Graphene are deposited on a nano-metric layer of Silica on a Si substrate. Every material in the nano-structure is modelled through the complex refractive index, the values of n and κ being obtained from both experimental data and theoretical models considered in [30]. The design permits the application of a gate voltage to modify the Graphene surface conductivity over the operating region of 10-300 THz. We compare this design and its operation for different gate voltages using Gold, identifying the differences of using Graphene under the influence of the same gate voltage.

The present dimensions follow the computational constraints associated with the thickness of the fractal that cannot be thicker than 3nm. A better design for the antenna is to scale it up by an order of magnitude or more while retaining the same thickness. Such a design will be able to scan with an order of magnitude smaller frequencies (10 times larger wavelengths). In this work, we model the material properties for wavelengths of 30 - 0.4 μm (10 - 750 THz). This approach differs from similar work in [31], for example, where Graphene is placed underneath a Copper patch, the fractal being on a 100 × 100 μm scale. Here, we consider a design which extends the frequency range of operation of a fractal antenna by introducing nano-features.

The plasmonic properties of a Graphene nano-antenna provide the ability to tune the antenna in the THz band. This is due to the Graphene surface conductivity that can be modified by

applying an electrostatic bias which changes the Fermi level [32]. In [33], Graphene is used as an electrically tuneable load in a nano-scale metal antenna gap. This permits an in-situ control of the antenna frequency. The Graphene patch antenna resonance frequency changes with its width and fractal type which are of growing interest because of their broad-band capabilities for applications using plasmonic metallic materials that generate emissions in the THz frequency (specifically 40 - 750 THz) [34].

6.1. Physical Model

In the model consider here, a fractal Graphene antenna is connected through a coaxial lumped port to a ground plane made of gold. A spherically Perfectly Matched Layer (PML) is then taken to include the Sierpinski triangle, the ground plane and the surrounding volume of air. The bottom of the Sierpinski triangle is flat and connected to a coaxial cable feed. The inner coaxial cable is taken to be gold surrounded by a SiO_2 outer coaxial casing, the ground plane also being taken to be made of gold.

As Graphene is a two-dimensional material, the volumetric conductivity is expressed in terms of the surface conductivity divided by the Graphene layer thickness Δ. The Sierpinski triangle is positioned on a layer of a SiO_2 dielectric on top of a semiconductor Si substrate. Additional matching parts are not required for using the antenna at higher-order resonances with the fractal structure given. The emission and propagation of EM waves is obtained by solving Equation (19) using a Finite Element Analysis (FEA). This spatial frequency domain model is appropriate under the assumption that all material properties are constant with respect to the field strength and the range of frequencies considered. The properties of the materials do not play any role in the macroscopic model, providing the conductivity is high enough to qualify as a PEC. However, at the nano-scale, the material models for n and κ selected in the design change the resonances of the antenna.

For the nano-metric dimensions considered, the second and third-order resonances of the small structures are placed at 320 and 600 THz [29] and we study the case for 10 -1000 THz. In regard to the material properties, for the case of Gold, experimental values for n and κ are provided for different configurations (films of different thickness, evaporated gold, template stripped gold, single-crystal gold) over the range of wavelength 0.3-25 μm [35], [36]. For Silicon, values of n and κ are obtained over the range 0.2-1.45 μm from [37] and [38]. In the case of Graphene, experimental measurements of n and κ are available in the region 0.15-0.95 μm from [28]. These values depend on the Graphene thickness and the substrate.

6.2. Example Results

Example results of the simulations are given in Figure 9 which shows the finite element model for the Sierpinski patch antenna and the Global S parameter for a THz frequency range. In this example, three resonances are found at 35, 110 and 215 THz, the most dominant resonance being for 215 THz. Figure 10 shows the electric field emissions in the far-field at these three resonant frequencies. These distributions are similar to those that would be achieved by a radiator modelled as a PEC except that lower resonance frequencies would be observed due to the properties of the material and structure of the antenna. Depending on the values of n and κ of the material selected for the radiator and the ground plane, these characteristics are changed at the nano-scale.

The thickness of Graphene influences the tuneable characteristics of the antenna and current simulations are dictated by the thickness of the Graphene patch being less than 3 nm. . This determines the minimum size of the mesh for modelling the fractal which must be a fraction of the thickness. To keep the number of mesh elements to a minimum, the dimensions of the antenna have been kept to a minimum. This is the reason for using the THz range in the FEA to generate the example results given in Figures 9 and 10.

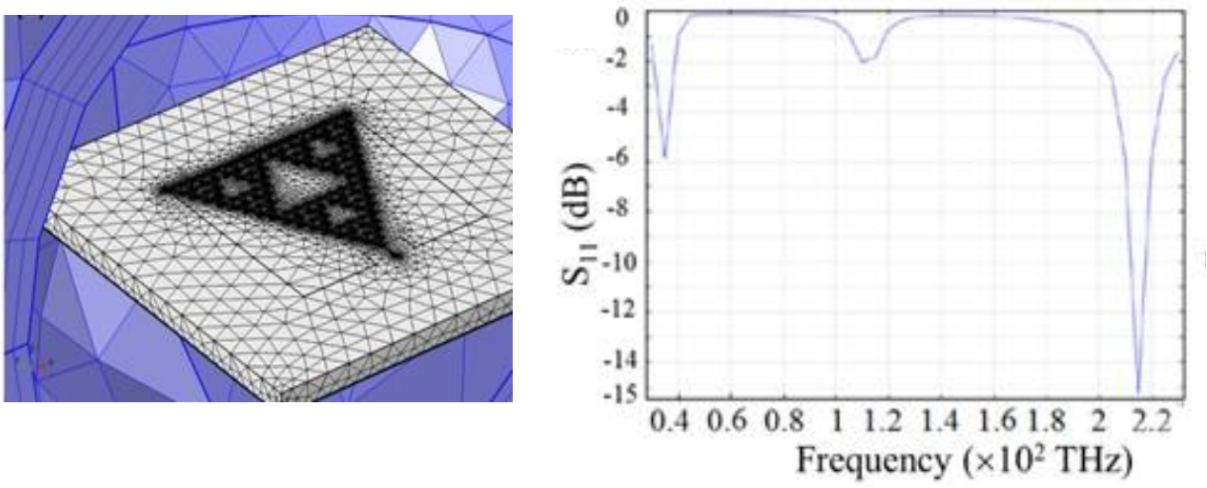

Figure 9. Example simulation for the Sierpinski triangle antenna model (left) showing the Global S-parameter (i.e. S_{11} which is the first element of the S-matrix) for a THz frequency range with three resonances at 35, 110 and 215 THz (right).

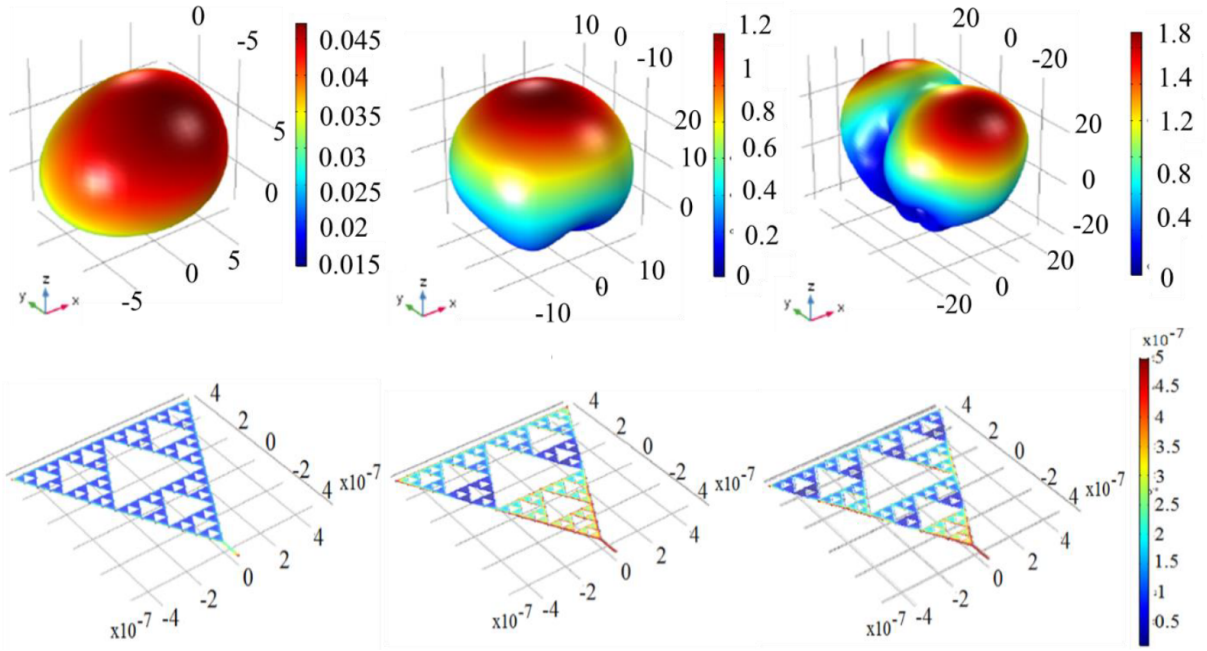

Figure 10. Far electric-field emission patterns (above) and surface electric-field distributions (below) for the Sierpinski fractal patch antenna and the three resonant frequencies, namely, 35, 110 and 215 THz (left to right, respectively).

By further scaling the antenna to operate in the frequency range 10-120 THz, for example, Graphene may have the advantage of being able to tune the refractive index (surface conductivity) if the thickness is approximated to be a single layer (or a few layers) by applying

a voltage across the layer and substrates.

The opportunity to model the properties of a Graphene antenna relies on special conditions to be enforced for the current density within the radiator. This can be accomplished by evaluating the complex permittivity of Graphene as the frequency and other parameters are varied and treating the film thickness as an impedance boundary that establishes a relationship between the currents flowing on the film surfaces. This increases the number of degrees of freedom and computational complexity, but, in this way, the total losses through the film can be computed with a more computationally stable discretisation. Moreover, nano-scale effects such as interface roughness can be introduced, evaluated, and correlated with experimental evidence. Hence, back-to-back modelling coupled with experimental activities are necessary to further progress the design of such an antenna.

The example radiation field patterns given in Figures 10 do not exhibit the fine structures associated with the fractal electric fields that will be formed in the far-field as discussed in Section 3.3. This is because of the resolution associated with simulated emissions that are limited within the context of the FEA simulations that have been undertaken.

7. THz Sources using Graphene

Technologies for generating THz sources have been available for many years and include vacuum electronics (the backward wave oscillator) and solid state electronics [39]. For micro- and nano-scale antennas, existing technologies are not suitable as this has a synergy to using a cavity magnetron designed for a microwave oven to feed a patch antenna in a mobile phone, for example. The solution to this problem is to consider Graphene itself as a material to generate a THz source and then integrate that source into a fractal Graphene antenna. To consider how this may be accomplished, the electron fluid model for the delocalised electrons on a Graphene surface as discussed in Section 4 needs to be revisited.

7.1. Electron Fluid Model

Consider the surface of Grphene to be composed of an assembly of electron clouds that collectively constitute an electron fluid. Because the electron clouds are composed of relativistic electrons we refer to this fluid as a Dirac fluid. The fluid represents a negatively charged surface upon which electrons (taken to be introduced by a source) are 'free' to move. For a Graphene patch antenna that is activated by a harmonic source, the electron fluid can then be taken to oscillate at a rate that is compatible with the frequency of the source. The oscillating electrons from which the fluid is composed then generate an EM field at the surface of the Graphene patch. An important feature of this model for a Graphene antenna (fractal or otherwise) is that the energy of the EM emission will not be effected by the frequency of the source if and only if the conductivity of the Graphene varies inversely with the frequency which is the case for $\omega\tau >> 1$ in the THz spectrum assuming a Drude model for the conductivity. In this case, Equation (14) can be taken to be valid for any frequency and thus, for an infinitely thin model, the electric field pattern generated by the patch is determined by the two-dimensional Fourier transform of the patch (as explored in Section 2.5) at any and all frequencies. This is an important reason as to why, on a micro- and nano-scale, Graphene antennas are required for the generation of THz EM fields.

7.2. Graphene THz Resonator

Like any other fluid, an electron fluid can support waves. In the case of Graphene, if an oscillating electric field is present on the surface that is parallel to that surface, then the electron fluid will start to oscillate at the same frequency to produce what is known as plasmon waves, the delocalised electrons in the fluid being, in effect, free negatively charges ions - a cold and strictly negatively charged plasma. So how can we force the electron fluid to oscillate at the

THz range? The answer is to apply an EM field in which the electric field oscillates at the required frequency, namely, in the far infrared (IR) region. This principle is called optical, or more specifically, IR pumping. The far infrared is any radiation with a wavelength of $\sim$ 15 μm to 1 mm (corresponding to a range of about 20 THz to 300 GHz) and is the long wavelength side of the far IR spectrum which overlaps with the THz spectrum.

Suppose we consider a Graphene ribbon mounted on a neutral dielectric substrate and attached to a source (of electrons) and a drain. Taking any plasmon wave motion of the electron fluid between source and drain to be linear, the system will possess a natural frequency that will depends on the length of the ribbon. If the plasmon waves are then optically pumped using an electric field oscillating at a frequency that is the same as this natural frequency, then a resonance will occur. The resonance will produce a standing plasmon wave over the extent of the Graphene strip giving a resonant 'photo-current' which in practice, requires the application of an IR laser. This photo-current will then induce an alternating current in any feed established between the source and drain, a feed that is connected (in a fully integrated sense) to a Graphene (fractal) antenna to generate a THz self-affine EM field. This is the principle by which Graphene can be used to source a fractal Graphene antenna through the stimulated emission of THz radiation with IR-pumping as illustrated schematically in Figure 11.

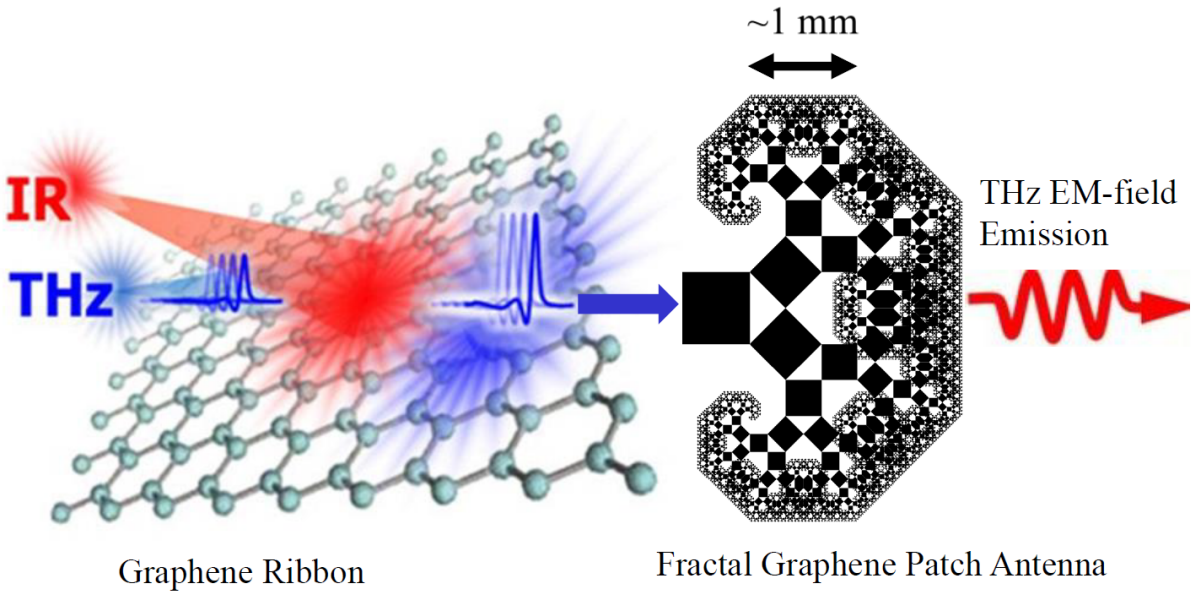

Figure 11. Schematic illustration of a Graphene THz resonator using IR-pumping to source a fractal Graphene antenna.

7.3. Modulation for Optimal Communication

The principle of using a Graphane ribbon to produce a THz resonator discussed in the previous section does not include the issue of how the THz source should be modulated so that information can be communicated in binary form, i.e. as s sequence of pulses, for example. The physics associated with modulating THz radiation from a Graphene source is the subject of current research and lies beyond the scope of this publication. However, the type of modulation that should ideally be applied in order to provide an optimal communications system can be specified. This is because:

(i) efficient micro- and nano-scale methods to generate powerful signals in THz range do not as yet exist thereby limiting THz communication systems to the near field $\sim$ meters;
(ii) the emission and reception of low power THz signals will be subject to distortion by background THz noise, leading to large bit error rates.

Studies on the characteristics of the background noise in the THz range will be undertaken in conjunction with the growth of THz communications systems in the future. However, the key issue is that points (i) and (ii) above necessitate the use of chirplet modulation.

In communications engineering, chirplet modulation has been implemented in a wide range of applications which have their origins in work dating back to the 1950s and 1960s, in particular, the invention and patenting of chirp pulse based communications (e.g. [40], [41]) and forms part of the wireless telecommunications IEEE standards [42]. Chirplet modulation provides an optimal solution to the communication of information through noise. This is why it is used in low power systems where background noise is a major source of bit errors including the noise generated by multiple reflections from the environment in which the system is used (e.g. enclosed spaces). An example of this is 'Bluetooth', a wireless technology standard used for exchanging data between fixed and mobile devices over short distances using short-wavelength radio waves from 2.402 GHz to 2.480 GHz, and, for building personal area networks. It can be shown that, of all the modulation techniques that are currently available or can be conceived, chirplet modulation will always provide the optimal solution for the communication of binary information through noisy channels [43]. Thus, in the development of future THz modulation technologies using micro- and nano-scale Graphene sources, the focus should be on the generation of chirplet modulation/demodulation methods. The best approach to the realisation of THz chirplet modulation is the basis for current and future research.

8. Summary

The principal purpose of this paper has been to investigate the basic physics associated with:

- using a Graphene ribbon to create a THz resonator;
- using a Graphene fractal patch antenna to emit and receive THz radiation.

The physical size of the resonator and radiator is taken to be on the micro- and nano-scales and thereby to yield low power systems that are only suitable for communications in the near field (a few meters at most) but capable of transferring binary data at a rate of Terabits per second using chirplet modulation (assuming the technology for this form a modulation can be realised).

The purpose of developing a Graphene resonator using IR-pumping it to provide a miniature THz source whose physical size and output power is compatible with that of a (patch) antenna radiating a THz EM field (with wavelength on the scale of nm-μm). The purpose of making the antenna from Graphene is because the material is the most (room temperature) conductive material of all and the purpose of using a fractal Graphene antenna is to create a communications system that can operate over many frequency channels.

Under the condition that Graphene adheres to a Drude model for its conductivity and that $\omega\tau >> 1$, the basic model for the emission of a scalar electric field is determined by Equation (14), under the condition that $\nabla \cdot \mathbf{E} = 0$ (and $\epsilon_r = 1$). For an infinitely thin patch, the far-field scalar electric field radiated by the patch is then determined by the (two-dimensional) Fourier transform of the source term which is independent of the frequency and determined solely by the geometrical structure associated with the current density. In this case, for a fractal patch antenna with a fractal dimension of $D \in (1, 2)$, the electric field is given by the Fourier transform of the fractal. In this context, a study on the Fourier transformation of fractals with $D \in (1, 2)$ is required. This is an aspect of fractal geometry that does not appear to have been researched in any significant depth and raises some interesting questions in regard to spectral properties of fractals in general as briefly considered in Section 3.3.

For the case when the Graphene is taken to have a relative permittivity $\epsilon_r > 1$ (which for Graphite is approximately 2.5), Equation (14) must be extended to the form

$$(\nabla^2 + k^2\epsilon_r)E(\mathbf{r}, k) = -J(\mathbf{r}) \tag{20}$$

where, for an applied electric field with amplitude E_0 that is used to generate the (oscillating) current density in the antenna, $J = \mu_0 ne^2 E_0/m \sim 30.45E_0$.

In terms of developing field models that are less conditional, we have considered Equation (19) and presented some example simulations based on a FEA solution to this equation. However, such simulations are currently limited to relatively low resolution models for the fractal. Hence, the far field self-affine radiation field patterns are not resolved in the simulations that have been undertaken to date and presented in this work. The model must be carefully revised to simulate fractal Graphene antennas by using externally performed simulations for the conditions to be enforced in the FEA of Equation (19). It also needs to be evaluated in regard to the relative simplicity of Equation (20) using semi-analytic solutions relative to Equation (19) using FEA.

9. Conclusions

The development of THz communications technology is at the forefront of IT and is an example of a disruptive technology that is set to revolutionise the quantity of digital information in wireless communications and nano-networks. On the basis of the study given in Section 3, we have shown that fractal patch antennas generate fractal EM field patterns in the far field. These field patterns allow for multiple frequency bands to be established and in this context, a fractal antenna may be considered to be a number of antennas in one as illustrated in Figure 6.

We have concluded that a Drude-type model for the conductivity of Graphene is valid. The critical point, is that, if the conductivity is taken to scale inversely with the frequency, then the EM field radiated by a Graphene antenna becomes frequency independent. While further investigations are required on the validity of this scaling relationship using semi-classical and quantum conductivity models of the type considered in Section 5, the general consensus of opinion is that for very high frequencies, the inverse frequency scaling relationship holds reasonably well. Thus, for a Graphene patch antenna, it should be expected that the strength of the field emission is frequency independent.

The electron (Dirac) fluid model described in Section 7.1 provides a useful, if a rather naive physical picture of how Graphene radiates an EM field. The fluid can be considered to oscillate at the same frequency as an applied electric field generated between a source and drain. Similarly, the fluid will oscillate when induced to do so by a incident EM field (the case for a receiving antenna). This is of course the same principle associated with any conductor. However, in a 'normal conductor' the delocalised electrons are significantly more localised than they are in Graphene and are not Fermionic. Because of the special properties of the electrons and their association with a Fermionic fluid, they are often referred to a Graphon's in order to differentiate their properties from plasmon's in other materials. Thus, Graphon's behave like a Dirac fluid and when pumped by an IR laser can be used to establish a resonance in a Graphene ribbon constrained by the physical micro-distance between the source and drain. It is this principle which provides the basis of using Graphene as a THz source.

10. Future Directions

The paper has introduced a number of issues that provide the basis for questions that will drive a range of specific research initiatives. We now consider some examples of such research themes.

10.1. Theoretical Issues

The reader is encouraged to consider the following:

(i) Since the EM far field emission generated by a fractal patch antenna is self-affine, then it is required to investigate what type of fractal antenna should be chosen to optimize the multi-bandwidth properties of a receiver and what type of fractal antenna will produce an EM field which has the same fractal structure. This involves an analysis of fractals in the frequency domain for which remarkably, there appears to be little information [44].

(ii) Given that for a micro-Graphene THz source (with a low power output), the antenna will only be operable in the near field, it is necessary to study the near field emission patterns (in the Fresnel zone) compounded in Equation (9). For the case of an infinitely thin patch antenna model, this will include a study of the field patterns produced by the convolution of $\exp(i\alpha r^2)$, $\mathbf{r} \in \mathbb{R}^2$ with a fractal for $D \in (1, 2)$, an area of interest for which the authors are unaware of any current studies (based on the available open literature).

(iii) The low power rating of the antennas considered necessitates the use of constructing arrays consisting of a regular (or possibly fractal) distribution of individual antennas. Modelling the field patterns of such arrays has not been considered in this work and requires the near field pattern of the array to be analysed through the application of Equation (7). It may then be of value to consider the characteristics of the far field radiation pattern obtained from an array that is itself characterised by a fractal structure, e.g. an antenna of the type shown in Figure 11 where each square component is itself a Graphene fractal.

(iv) A freely suspended Graphene membrane is always partially crumpled because two-dimensional crystals in a three-dimensional space can not be flat due to bending instabilities and thermally induced perturbations. According to the Mermin-Wagner Theorem, 'in one- and two-dimensions, continuous symmetries cannot be spontaneously broken at finite temperatures in systems with sufficiently short-range interactions' [45]. Long-wavelength fluctuations destroy the long-range order of two-dimensional crystals [46] and hence, two-dimensional membranes embedded in a three-dimensional space have a tendency to become crumpled. The spatial characteristics of Graphene therefore include intrinsic defects such as warping, crumpling and rippling. Graphene ripples have various sizes, have a broad distribution and power-law correlation functions of normals together with some typical scale lengths due to the intrinsic tendency of carbon to be bonded. Consequently, there have been a variety of attempts to model the Graphene defects and the defect dynamics of the material [47] and requires further investigations in regard to the efficiency of fractal patch antennas composed of Graphene.

(v) The deformation of Graphene effects the properties of the material and it is therefore important to incorporate this phenomenon in a model for electron transport [48]. This includes the use of fractal surface models on the basis that the deformation of Graphene might be expected to have random self-affine structures [49]. The effect on the conductivity is to change the inverse frequency scaling law associated with a Drude type model to one where the conductivity is proportional to $1/\omega^{\alpha}$, $\alpha > 1$ (for $\omega >> 1$). For the evaluation of the conductivity using quantum electron scattering, a fractal crumpling model can be undertaken by replacing the periodic potential $V(\mathbf{r} + \mathbf{R})$ with $V(\mathbf{r} + \mathbf{R})f(\mathbf{r})$ where $f(\mathbf{r})$ is the (random) fractal, that, unlike the potential, is not periodic. For $\mathbf{r} \in \mathbb{R}^1$, the reflection coefficient (see Appendix B.3) is determined by (using the product theorem)

$$R(k/2) = \frac{i}{k} \int_{-\infty}^{\infty} f(x)V(x + X) \exp(-ikx)dx = \frac{i}{2\pi k}[F(k) \otimes \widetilde{V}(k) \exp(ikX)]$$

where $F(k)$ and $\widetilde{V}(k)$ are the (one-dimensional) Fourier transforms of $f(x)$ and $V(x)$, respectively. Thus, for the scaling relationship associated with Equation (13), we obtain

the asymptotic result

$$R(k/2) \sim \frac{2i}{2\pi k} \int_{-\infty}^{\infty} \frac{(\gamma + \ln \mid \xi \mid) \exp(i\xi X) d\xi}{\mid k - \xi \mid^q} = \frac{1}{ik \mid k \mid^q} \frac{1}{\mid X \mid}, \; k \to \infty$$

and we can expect the QC to scale with frequency according to $\sim 1/\omega^{1+q}, \; \omega > 0$ in the high frequency limit.

(vi) The delocalised electrons in Graphene are taken to be relativistic which is the reason why a large population density of Graphon's can be taken to form a Dirac fluid. However, it is arguable that the speed of these electrons ($\sim 70\%$ light speed) is not so close to the speed of light as to consider them to be fully relativistic particles. They therefore represent an interesting case when neither a relativistic or a non-relativistic model is ideal and fall into a semi-relativistic regime. A phenomenological (one-dimensional) model for this case has been considered using the equation [50]

$$-i^{1+\alpha} \partial_t^{(1+\alpha)} \Psi(x,t) = -\alpha m^2 \Psi(x,t) + \left(\frac{1}{2m}\right)^{1-\alpha} \partial_x^2 \Psi(x,t)$$

where, as $\alpha \to 0$ and as $\alpha \to 1$, the Schrödinger and the Klein-Gordon equations are recovered, respectively. The wave function Ψ describes spin-less particles and it can be shown that the temporal property of a mass-less Graphon propagator (the time dependent Green's function G) is characterized by $\mid G(0,t) \mid^2 \sim 1/t^{1-\alpha}, \; t > 0$. This scaling function is the kernel of the fractional (Riemann-Liouville) integral which is scale invariant. Thus, it may therefore be expected that Graphon propagator's are time fractals.

10.2. Engineering Issues

Issues associated with the engineering of a micro- and nano-scale fractal antennas have not been considered in this paper but, in practice, the antenna would be cut using e-beam lithography after it has been mounted on a neutral substrate. To do this effectively, it is necessary to minimise crumpling when the Graphene is both mounted and then cut with a e-beam. In regard to the latter case, it is required to ascertain the physical scale limits to which a fractal can be cut, subject to maintaining (electrical) connectivity throughout the fractal Graphene patch. Once fabricated, the fractal Graphene patch will need to be inspected. For this purpose, commercially available technology that includes dual E-Beam Lithography (EBL) and Scanning Electron Microscopy (SEM) will be required such as the 'PIONEER Two' nano-fabrication, for example, which combines all maximum performance elements for specialised EBL and SEM into a single comprehensive turnkey system [51].

Irrespective of the technologies that are utilised, to fabricate such an antenna, research on the optimisation of the product is required to provide answers to the following example questions:

- What is the size of mono-layer Graphene that can be used?
- what are the best fractal patch types to use in terms of energy output and the multiple frequency bands expected?
- given a specific fractal type, what is the smallest scale to which the Graphene can be cut without leading to discontinuities and crumpling defects that make the efficiency of the antenna at that scale unacceptable?

In regard to engineering a Graphene resonator by IR laser pumping, research is still at an early stage and the problem of how to provide a resonator that can output chirplet modulated pulses is an area of research that does not appear to have been initiated to date.

10.3. Applications

The quest to fill the 'THz gap' is on-going as it provides one of the last great leaps forward in the field of wireless communications. Those who master the technology first will have short range communications at Tbps in a band that no one else can 'listen in to', until such a time as the 'others' catch up. The applications of the technology is limited only by the near field condition. Given this condition, multi-band Tbps wireless communications will provide a level of data transfer that is unprecedented in the provision of new nano-networks. Such communications systems would not necessarily need to include data encryption and would therefore have significant military applications in regard to localised mobile communications.

Acknowledgments

The authors acknowledge the support of their respective universities and research institutes, to Leonardo Aerospace, Defence and Security, and, in the case of Jonathan Blackledge, the UK Ministry of Defence. The concept of a nano-scale fractal Graphene antenna for THz communications was originally conceived by Jonathan Blackledge and Alberto Boretti through their collaboration at the Military Technological College, Oman.

Appendix A. Intermediate and Far Field Representations of the Electric Field

Given Equation (5), the expressions for the electric field in both the intermediate and far fields are predicated on the binomial expansion of $|\,\mathbf{r}-\mathbf{s}\,|$, namely

$$|\,\mathbf{r}-\mathbf{s}\,| = r\left(1-\frac{2\mathbf{r}\cdot\mathbf{s}}{r^2}+\frac{s^2}{r^2}\right)^{\frac{1}{2}} \simeq r-\frac{\mathbf{r}\cdot\mathbf{s}}{r}+\frac{s^2}{2r}$$

Thus, noting that

$$\frac{r}{2}-\frac{\mathbf{r}\cdot\mathbf{s}}{r}+\frac{s^2}{2r}=\frac{1}{2r}\,|\,\mathbf{r}-\mathbf{s}\,|^2 \Rightarrow\; r-\frac{\mathbf{r}\cdot\mathbf{s}}{r}+\frac{s^2}{2r}=\frac{1}{2r}\,|\,\mathbf{r}-\mathbf{s}\,|^2+\frac{r}{2}$$

we can then write an approximation to Equation (5) given by

$$E(\mathbf{r},k)=\frac{ikz_0}{4\pi r}\exp(ikr/2)\int\limits_{\mathbf{s}\in\mathbb{R}^3}\exp(i\alpha\,|\,\mathbf{r}-\mathbf{s}\,|^2)J(\mathbf{s})d^3\mathbf{s}=\frac{ikz_0}{4\pi r}\exp(ikr/2)K(\mathbf{r},k)$$

where

$$K(\mathbf{r},k)=\exp(i\alpha r^2)\otimes J(\mathbf{r})$$

and $\alpha = k/2r$. This result provides an expression for the electric field in the Fresnel or intermediate zone. It is an expression for the electric field that occurs at some distance away from the spatial domain in which the current density exists such that $s^2/r^2 << 1$ and is characterised by the convolution with quadratic phase-only function $\exp(i\alpha r^2)$.

If the electric field generated by the current density is taken to be a large distance away from the current density such that $s/r << 1$ then we can consider the case when

$$|\,\mathbf{r}-\mathbf{s}\,| \simeq r\left(1-\frac{2\mathbf{r}\cdot\mathbf{s}}{r^2}\right)^{\frac{1}{2}} \sim r-\frac{\mathbf{r}\cdot\mathbf{s}}{r}$$

from which it follows that a further approximation for the electric field is obtained and Equation (5) is reduced to the asymptotic form

$$E(\mathbf{r},k)=\frac{ikz_0}{4\pi r}\exp(ikr)\widetilde{J}(\mathbf{k}),\; r\to\infty$$

where, with $\mathcal{F}_3$ denoting the three-dimensional Fourier transform,

$$\widetilde{J}(\mathbf{k}) = \mathcal{F}_3[J(\mathbf{s})] = \int\limits_{\mathbf{s}\in\mathbb{R}^3} \exp(-i\mathbf{k}\cdot\mathbf{s})J(\mathbf{s})d^3\mathbf{s},\ \mathbf{k} = k\hat{\mathbf{n}},\ \hat{\mathbf{n}} = \frac{\mathbf{r}}{r}$$

This is an expression for the electric field in the far field of Fourier plane because it is characterised by the Fourier transform of the current density.

Appendix B. Weak Scattering Approximations for a Coulomb Potential for $\mathbf{r} \in \mathbb{R}^n$

It is well known that, under the Born approximation, and, for an incident (unit amplitude) plane wave, Equation (17) reduces to a Fourier transform representation for the scattering amplitude in the far-field [24].

Appendix B.1. Analysis for $\mathbf{r} \in \mathbb{R}^2$

For the two-dimensional case,

$$\psi_s(r, \mathbf{K}) = -\frac{\exp(i\pi/4)\exp(ikr)}{\sqrt{8\pi r}}A(\mathbf{K}),\ r \to \infty$$

where

$$A(\mathbf{K}) = \frac{1}{\sqrt{k}}\int\limits_{-\infty}^{\infty} V(\mathbf{r})\exp(-i\mathbf{K}\cdot\mathbf{r})d^2\mathbf{r},\ \mathbf{K} = k(\hat{\mathbf{n}}_s - \hat{\mathbf{n}}_i)$$

The unit vectors $\hat{\mathbf{n}}_i$ and $\hat{\mathbf{n}}_s$ denote the directions of the incident and scattered electrons (in the Graphene plane), respectively.

The electron scattering potential (i.e. the electron clouds associated with each hexagonal cell in the lattice of Graphene) is regularly spaced in the plane; it is a periodic potential. Thus, the scattering potential is given by $V(\mathbf{r} + \mathbf{R})$ where $\mathbf{R}$ is the lattice vector, $R \equiv \mid \mathbf{R} \mid$ being the radial distance from the centre of one Graphene cell to another. Using the shift theorem, the scattering amplitude is therefore given by

$$A(\mathbf{K}) = \exp(i\mathbf{K}\cdot\mathbf{R})\frac{1}{\sqrt{k}}\int\limits_{-\infty}^{\infty} V(\mathbf{r})\exp(-i\mathbf{K}\cdot\mathbf{r})d^2\mathbf{r}$$

Thus, the effect of electron scattering in the Graphene plane can be investigated by evaluating the scattering cross-section for a single cell alone - the equivalent of Bloch's Theorem [25], [26].

Using polar coordinates (r, ϕ), the scattering amplitude becomes

$$A(\hat{\mathbf{n}}_s, \hat{\mathbf{n}}_i) = \frac{1}{\sqrt{k}}\int\limits_{-\pi}^{\pi}\int\limits_{0}^{\infty} V(\mathbf{r})\exp(-ik \mid \hat{\mathbf{n}}_s - \hat{\mathbf{n}}_i \mid r\cos\phi)rdrd\phi$$

where, for a scattering angle in the plane denoted by θ, $K = k \mid \hat{\mathbf{n}}_s - \hat{\mathbf{n}}_i \mid = 2k\sin(\theta/2)$. Thus, using the definition of a zero-order Bessel function J_0, we can write

$$A(K) = \frac{2\pi}{\sqrt{k}}\int\limits_{0}^{\infty} V(\mathbf{r})J_0(Kr)rdr \ \text{ where } \ J_0(Kr) = \frac{1}{2\pi}\int\limits_{-\pi}^{\pi}\exp(-iKr\cos\phi)d\phi$$

For a radially symmetric scattering potential $V(r)$, the scattering amplitude is then determined by the zero-order Hankel transform, i.e.

$$A(K) = \frac{2\pi}{\sqrt{k}}\mathcal{H}_0(K) \text{ where } \mathcal{H}_0(K) = \int_0^\infty V(r)J_0(Kr)rdr$$

Consider the case when the electron-electron scattering over the plane of mono-layer Graphene is characterised by a Coulomb potential for a point charge when $V(r) = e/r$. In this case, the Hankel transform is given by e/K, and the scattering amplitude is

$$A(\theta, k) = \frac{\pi e}{k^{3/2}\sin(\theta/2)}$$

This result illustrates that the scattering cross-section is dominated by forward scattering when $\theta = 0$ and that the quantum conductivity is proportional to $1/\omega^{3/2}$, $\omega > 0$.

Appendix B.2. Analysis for $\mathbf{r} \in \mathbb{R}^3$
Repeating the analysis provided in the previous section for the case when $\mathbf{r} \in \mathbb{R}^3$ for a spherically symmetric potential (and spherical polar coordinates), the scattering amplitude becomes

$$A(\theta) = \frac{2\pi}{k\sin(\theta/2)}\int_0^\infty \sin[2kr\sin(\theta/2)]V(r)rdr$$

In this case, if we use a Coulomb potential, the integrand does not converge as $r \to \infty$. To solve this problem, we consider the screened Coulomb potential $V(r) = e\exp(-ar)/r$, $a > 0$ for which the integral can be evaluated and let $a \to 0$, the scattering amplitude being given by

$$A(\theta) = \frac{\pi e}{k^2\sin^2(\theta/2)}\left(1 + \frac{a^2}{[2k\sin(\theta/2)]^2}\right)^{-1} \simeq \frac{\pi e}{k^2\sin^2(\theta/2)},\ a \to 0$$

It is then clear that quantum conductivity is proportional to $1/\omega^2$, the angular dependence of the scattering cross-section being characteristic of Rutherford scattering [27].

Appendix B.3. Analysis for $\mathbf{r} \in \mathbb{R}^1$
In one-dimension, the scattered field (specifically the back-scattered field determined by 'Reflection Coefficient' R) is given by

$$\psi_s(x,k) = -\exp(ikx)R(k) \text{ where } R(k) = \frac{i}{2k}\int_{-\infty}^\infty V(x)\exp(-2ikx)dx,\ x \to \infty$$

Thus, for a Coulomb potential, when $V(x) = e/\mid x \mid$, and, noting that

$$\int_{-\infty}^\infty \frac{\exp(-ikx)dx}{\mid x \mid} = -2(\gamma + \ln \mid k \mid)$$

where $\gamma \simeq 0.57721$ is the Euler-Mascheroni constant, the Reflection Coefficient is given by

$$R(k) = \frac{ie}{k}(\gamma + \ln \mid 2k \mid) \Rightarrow \mid \psi_s \mid^2 = \frac{\hbar e^2}{2m\omega}\left(6.1489 + \frac{1}{2}\ln\omega\right)^2 \sim \frac{3\hbar e^2}{m\omega},\ \omega \to \infty$$

This result includes a frequency scaling relationship compatible with the Drude model discussed in Section 5.1. The 'Conductance Quantum' (i.e. the quantized unit of electrical conductance) is given by $e^2/\pi\hbar$ S, and thus, for an electron number density n (i.e. the number of electrons per unit length) we can write the electrical conductivity as

$$\sigma = \frac{n}{\pi\hbar} \mid \psi_s \mid^2 \sim \frac{3ne^2}{\pi m\omega} \text{ S/m}$$

For a Graphene ribbon in which the length of the lattice is significantly larger than its width, we may expect a one-dimensional model to be more significant. This argument also applies to the fine structures associated with a fractal composed of Graphene.

References

[1] Wallace P R 1947 The Band Theory of Graphite, *Physical Review* **71**(9) 622–634 https://journals.aps.org/pr/abstract/10.1103/PhysRev.71.622
[2] Baird D Hughes R I G and Nordmann A (Eds.) 1998 *Heinrich Hertz: Classical Physicist, Modern Philosopher* Springer-Verlag, ISBN 0-7923-4653-X
[3] Maxwell J C 1865 A Dynamical Theory of the Electromagnetic Field, *Philosophical Transactions of the Royal Society of London* **55** 459–512 https://royalsocietypublishing.org/doi/10.1098/rstl.1865.0008
[4] Sizov F and Rogalski A 2010 Review of THz Detectors *Progress in Quantum Electronics* Elsevier **34** 278–347
[5] Novoselov K S, Geim A K, Morozov S V, Jiang D, Katsnelson M I, Grigorieva I V, Dubonos S V and Firsov A A 2005. Two-dimensional Gas of Massless Dirac Fermions in Graphene. *Nature* **438**(7065) 197–200 https://www.nature.com/articles/nature04233
[6] Mikhail M et al Optical Pumping in Graphene-based Terahertz/Far-infrared Superluminescent and Laser Heterostructures with Graded-gap Black-P_xAs_{1-x} Absorbing-cooling Layers 2019 *Optical Engineering* **59**(6) 061606 https://doi.org/10.1117/1.OE.59.6.061606
[7] Ju et al 2011 Graphene Plasmonics for Tunable Terahertz Metamaterials *Nat Nano* **6** 630-634
[8] Llatser et al 2012 Graphene-based Nano-patch Antenna for Terahertz Radiation, *Photonics and Nanostructures - Fundamentals and Applications* **10** 353-358
[9] Zakrajsek et al 2016 Lithographically Defined Plasmonic Graphene Antennas for Terahertz-band Communication, *IEEE Antennas and Wireless Propagation Letters* **15** 1553-1556
[10] Evans G Blackledge J and Yardley P 1999 *Analytic Methods for Partial Differential Equations* Springer Undergraduate Mathematics Series (Springer) ISBN: 978-3-540-76124-2
[11] Khan A Nema R 2012 Analysis of Five Different Dielectric Substrates on Microstrip Patch Antenna *International Journal of Computer Applications* **55**(14) 40-47 https://research.ijcaonline.org/volume55/number14/pxc3882905.pdf
[12] Turner M Blackledge J and Andrews P 1998 *Fractal Geometry in Digital Imaging* (Academic Press), ISBN-13: 978-0127039701
[13] Geim A and Novoselov K 2007 The Rise of Graphene *Nat Mater* **6** 183-191
[14] Graphene (The University of Manchester) https://www.graphene.manchester.ac.uk/about/
[15] Katsnelson K 2012 *Graphene: Carbon in Two Dimensions* (Cambridge University Press) ISBN: 978-1107375802
[16] Sikesb et al 2008 Ultrahigh Electron Mobility in Suspended Graphene *Solid State Communications* (Elsevier) **146**(9–10) 351–355
[17] Brey L and Fertig H 2006 Electronic States of Graphene Nano-ribbons Studied with the Dirac Equation *Phys. Rev. B* **73** 235-411
[18] Bardarson et al 2007, One-Parameter Scaling at the Dirac Point in Graphene *Phys. Rev. Lett.* **99** 106-801
[19] , Gi N 2011 *Relativistic Dynamics and Dirac Particles in Graphene* PhD Thesis Massachusetts Institute of Technology
[20] Drude P 1900 Zur Elektronentheorie der Metalle, *Annalen der Physik* **306**(3) 566–613
[21] Drude P 1900 Zur Elektronentheorie der Metalle II: Teil. Galvanomagnetische und thermomagnetische Effecte, *Annalen der Physik* **308**(11) 369–402
[22] Fang et al 2007 Carrier Statistics and Quantum Capacitance of Graphene Sheets and Ribbons *Appl. Phys. Lett.* **91** 92-109
[23] Hanson G W 2008 Dyadic Green's Functions and Guided Surface waves for a Surface Conductivity Model of Graphene, *Journal of Applied Physics* **103**, 064302 https://doi.org/10.1063/1.2891452
[24] Blackledge J 2005 *Digital Image Processing: Mathematical and Computational Methods* Woodhead

Publishing Series in Electronic and Optical Materials (Woodhead Publishing) ISBN-13: 978-1898563495. https://arrow.tudublin.ie/engschelebk/3/
[25] Bloch F 1928 On the Quantum Mechanics of Electrons in Crystal Lattices *Zeitschrift für Physik* **52**(7–8) 555–600 https://link.springer.com/article/10.1007%2FBF01339455
[26] Kittel C 1996 *Introduction to Solid State Physics* Wiley ISBN 0-471-14286-7
[27] Rutherford E 1911 The Scattering of α and β Rays by Matter and the Structure of the Atom *Philosophical Magazine* **21**(6) 669-688
[28] Ochoa-Martinez et al 2015 Determination of a Refractive Index and an Extinction Coefficient of Standard Production of cvd-Graphene *Nanoscale* **7** 1491-1500
[29] Mishra R Ghatak R and Poddar D R 2008 Design Formula for Sierpinski Gasket Pre-fractal Planar-monopole Antennas [antenna designer's notebook] *IEEE Antennas and Propagation Magazine* **50** 104-107
[30] Boretti et al 2020 *A Preliminary Study of a Graphene Fractal Sierpinski Antenna*, 4th International Conference on Materials Engineering and Nano Sciences (ICMENS2020) Pattaya Thailand https://arrow.tudublin.ie/engscheleart/310/
[31] , Xu Y Hu J and Yin W 2013 *Design of a Novel Reconfigurable Sierpinski Fractal Graphene Antenna Operating at the Thz Band* IEEE Antennas and Propagation Society International Symposium (APSURSI) 574-575
[32] Jornet J and Akyildiz I 2013, Graphene-based Plasmonic Nano-antenna for Terahertz band Communication in Nano-networks, *IEEE Journal on Selected Areas in Communications* **31** 685-694
[33] Yao et al 2013 Broad Electrical Tuning of Graphene-loaded Plasmonic Antennas *Nano Letters* **13** 1257-1264
[34] Rosa L Sun K and Juodkazis S 2011 Sierpinski Fractal Plasmonic Nano-antennas *Physica Status Solidi* Rapid Research Letters **5** 175-177.
[35] Gao L Lemarchand F and Lequime M 2011 Comparison of Different Dispersion Models for Single Layer Optical Thin Film Index Determination *Thin Solid Films* **520** 501-509
[36] Olmon et al 2012 Optical Dielectric Function of Gold *Physical Review B* **86** 235147
[37] Green M 2008 Self-consistent Optical Parameters of Intrinsic Silicon at 300K Including Temperature Coefficients *Solar Energy Materials and Solar Cells* **92** 1305-1310.
[38] Chandler-Horowitz D and Amirtharaj P 2005 High-accuracy, Mid-infrared ($450\text{cm}^{-1} \leq \omega \leq 4000\text{cm}^{-1}$) Refractive Index Values of Silicon *Journal of Applied Physics* **97** 123526
[39] Gilmour A Klystrons 2011 *Traveling Wave Tubes, Magnetrons, Crossed-Field Amplifiers and Gyrotrons* (Artech House) 2ISBN 1608071855
[40] Darlington S 1954 *Chirp Pulse Transmission* US Patent 2678997
[41] Darlington S 1969 *Chirp Pulse Equalization*, US Patent 3618095
[42] IEEE Computer Society 2007 *IEEE Standard 802.15.4a-2007* https://ieeexplore.ieee.org/document/4299496
[43] Blackledge J 2020 On the Chirp Function, the Chirplet Transform and the Optimal Communication of Information, *IAENG International Journal of Applied Mathematics* **50**(2) 285-319 https://arrow.tudublin.ie/engscheleart2/218/
[44] Durable Scope 2020 *Frequency Analysis of Fractals with Fourier Transforms: Exploring the Characteristics of Various Fractals using Frequency Analysis Techniques* https://blog.durablescope.com/post/Analysis_of_Fractals_with_Fourier_Transform/
[45] Werner A 2010 *The Mermin-Wagner Theorem* http://itp.uni-frankfurt.de/~valenti/TALKS_BACHELOR/mermin-wagner.pdf
[46] Hohenberg P 1967 Existence of Long-range Order in One- and Two-Dimensions, *Phys. Rev. Vol.* **158**(2) 383-386
[47] Chen et al 2009 Raman Spectroscopy of Ripple Formation in Suspended Graphene *Nano Letters* **9**(12) 4172–4176
[48] Zwierzycki M 2012 Transport Properties of Rippled Graphene, *Acta Physica Polonica A* **121** 1246-1249
[49] Blackledge J and Rebow M 2014 Two-dimensional Schrodinger Scattering and Electron Transport in Graphene *International Journal for Pure and Applied Mathematics* **4**(8) 913-926. https://arrow.tudublin.ie/engscheleart2/108/
[50] Blackledge J and Babajanov B 2013 The Fractional Schrodinger-Klein-Gordon Equation and Intermediate Relativism, *International Journal for Pure and Applied Mathematics (Mathematica Aeterna)* **3**(8) 601 - 615 https://arrow.tudublin.ie/engscheleart2/76/
[51] Pioneer Two Electron Beam Lithography and Scanning Electron Microscope Imaging 2020 https://www.azonano.com/equipment-details.aspx?EquipID=1752